Identifying areas at risk of drought-induced tree mortality across South-Eastern Australia

Identifying areas at risk of drought-induced tree mortality across South-Eastern Australia

Martin G. De Kauwe[1,2,3]* Belinda E. Medlyn[4.], Anna M. Ukkola[1,5], Mengyuan Mu[1,2], Manon E. B. Sabot[1,2], Andrew J. Pitman[1,2], Patrick Meir[6,7.], Lucas Cernusak[8.], Sami W. Rifai[2], B. Choat[4.], David T. Tissue[4.], Chris J. Blackman[4.], Ximeng Li[4.], Michael Roderick[1,5] and Peter R. Briggs[9.]

[1.]ARC Centre of Excellence for Climate Extremes, Sydney, NSW 2052, Australia.

[2.]Climate Change Research Centre, University of New South Wales, Sydney, NSW 2052, Australia.

[3.]Evolution & Ecology Research Centre, University of New South Wales, Sydney, NSW 2052, Australia.

[4.]Hawkesbury Institute for the Environment, Western Sydney University, Locked Bag 1797, Penrith, NSW 2751, Australia

[5.]Research School of Earth Sciences, Australian National University, Canberra, ACT 2601, Australia

[6.]Research School of Biology, The Australian National University, Acton ACT 2601, Australia

[7.]School of Geosciences, University of Edinburgh, Edinburgh EH93ff United Kingdom

[8.]College of Science and Engineering, James Cook University, Cairns, Qld 4814, Australia

[9.]CSIRO Oceans and Atmosphere, Canberra, 2601, Australia

* *Corresponding author address*: Martin De Kauwe, Climate Change Research Centre, University of New South Wales, New South Wales 2052, Australia. E-mail: mdekauwe@gmail.com Phone: +61 2 9385 8481

Running head: *Predicting drought-induced tree mortality Keywords: cavitation resistance, drought tolerance, plant hydraulics, land surface model, Australia*

Keywords:

Word count: 8143/8000

Abstract

South-East Australia has recently been subjected to two of the worst droughts in the historical record (Millennium Drought, 2000–2009 and Big Dry, 2017–2019). Unfortunately, a lack of forest monitoring has made it difficult to determine whether widespread tree mortality has resulted from these droughts. Anecdotal observations suggest the Big Dry may have led to more significant tree mortality than the Millennium drought. Critically, to be able to robustly project future expected climate change effects on Australian vegetation, we need to be able to assess the vulnerability to drought of Australian trees. Here, we implemented a model of plant hydraulics into the Community Atmosphere Biosphere Land Exchange (CABLE) land surface model. We parameterised the drought response behaviour of five broad vegetation types, based on a common garden dry-down experiment with species originating across a rainfall gradient (188–1125 mm yr^{-1}) across South-East Australia. The new hydraulics model

significantly improved (~35–45 % reduction in root mean square error) CABLE's previous predictions of latent heat fluxes during periods of water stress at two eddy covariance sites in Australia. Landscape-scale predictions of the greatest percentage loss of hydraulic conductivity (PLC), 40–60 %, were broadly consistent with satellite estimates of regions of the greatest change in both droughts. In neither drought did CABLE predict that trees would have reached critical PLC in widespread areas (i.e. it projected a low mortality risk), although the model highlighted critical levels near the desert regions of South-East Australia where few trees live. Overall, our experimentally constrained model results imply significant resilience to drought conferred by hydraulic function, but also highlight critical data and scientific gaps. Our approach presents a promising avenue to integrate experimental data and make regional-scale predictions of potential drought-induced hydraulic failure.

Introduction

Australia is the driest inhabited continent, with the greatest inter-annual variability in rainfall, and is prone to severe multi-year droughts. Tree species that occur in this environment are well adapted to rainfall variability and extended drought periods (Myers & Neales, 1984; Stoneman, 1994; Arndt *et al.*, 2015), but it is nonetheless unclear whether they will continue to thrive as the climate changes. Some climate studies project more intense, longer lasting and more frequent droughts (Dai, 2013; Trenberth *et al.*, 2014; Cook *et al.*, 2015), although divergence in model projections of future regional precipitation patterns (Collins *et al.*, 2013) makes it difficult to determine how drought characteristics may change. Nevertheless, we can be certain that future drought episodes will occur against the widely predicted background of increasing air temperature in the immediate future (Reichstein *et al.*, 2013; Williams *et al.*, 2013; Trenberth *et al.*, 2014). Globally, projected changes in drought incidence are consistent with increased reports of severe drought events (Ciais *et al.*, 2005; Fensham *et al.*, 2009;

Phillips *et al.*, 2009; Allen *et al.*, 2015), declines in forest productivity linked to water limitations (Peñuelas *et al.*, 2011) and associated tree mortality (Breshears *et al.*, 2005; Anderegg *et al.*, 2013; Mitchell *et al.*, 2014).

In contrast to the apparent increasing global trend in drought-induced tree mortality, there have been relatively few reports of similar events in Australia. Mitchell *et al.* (2014) in their literature review found only 17 scientific reports of drought-related die-off events since 1891. The decadal (2000–2010) Millennium drought was the worst drought on record for South-East Australia (van Dijk *et al.*, 2013); Figures S1 and S2) and yet, Jiang *et al.* (2019), attempting to ground-truth remotely-sensed drought impacts, found only four locations where drought mortality was observed during the period. However, archival studies of newspaper reports during historical droughts, such as the Federation Drought (1891-1903), have found numerous observations of drought-related mortality (Fensham & Holman, 1999; Godfree *et al.*, 2019). This poses an important question: is widespread drought-induced mortality rare among Australian trees? Or simply under-reported?

Despite detailed reporting on the impacts of the Millennium drought on agriculture, hydrology and the economy (Carter & White, 2009; van Dijk *et al.*, 2013), there remains a striking gap in the quantification of drought impacts for Australia's tree species. This critical knowledge gap means that we do not know which species or forest types are most vulnerable, or what thresholds of drought stress are required to induce tree mortality among Australian species. Without this information, we are limited in our ability to develop or test a physiological understanding of the mechanisms that lead to tree die-off. As a result, we cannot robustly predict future drought vulnerability for Australian trees or predict changes in community species composition due to drought (Mueller *et al.*, 2005; Nepstad *et al.*, 2007; Ruthrof *et al.*, 2015). A better understanding of the required magnitude of water stress that

would invoke hydraulic failure and lead to mortality (Adams *et al.*, 2017) is urgently needed to comprehend the drought-tolerance of tree species, both within Australia and across the globe.

Based on current literature, it is unclear whether species occurring in mesic or xeric environments are most vulnerable to the impacts of drought, or if both environments are equally vulnerable (Choat *et al.*, 2012). We might hypothesise that species growing in more arid environments would be well adapted to water stress (i.e. greater xylem resilience to cavitation). By contrast, in mesic regions, climate variability is typically muted. As a result, ecological adaptions may be less plastic to stochastic drought (Arndt *et al.*, 2015; Jump *et al.*, 2017), as witnessed in the large Amazon rainforest droughts (Bittencourt *et al.*, 2020). Similarly, many studies have highlighted a greater drought sensitivity in larger trees, especially in particular taxa (Nepstad *et al.*, 2007; Phillips *et al.*, 2010; Rowland *et al.*, 2015; Bittencourt *et al.*, 2020), consistent with a hypothesis of greater drought stress in mesic species via the water transport system. Conversely, other studies have shown greater impacts of drought in drier environments (Ruiz-Benito *et al.*, 2014; Anderegg *et al.*, 2015), or for species growing at the edge of their distributions (Galiano *et al.*, 2010; Anderegg *et al.*, 2019). Many taller trees could also have invested more heavily in a deeper rooting structure (Fan *et al.*, 2017), which implies resilience may be at odds with apparent greater drought sensitivity. Overall, there is no clear consensus among studies as to where, when, and which species are most vulnerable to the impacts of drought

One way to estimate drought mortality thresholds is to use empirical approaches based on mortality observations. In the southwestern United States, Anderegg *et al.* (2015) successfully demonstrated a link between observed mortality of *Populus tremuloides* and a climatic water deficit metric (the difference between potential and actual evapotranspiration), then inferred

widespread future mortality based on coupled climate model projections and their observed mortality threshold. Where extensive monitoring networks exist (e.g. many countries in Europe), tree mortality has been empirically linked to climate variability (anomalies in temperature and precipitation) and tree age (Neumann *et al.*, 2017). In Australia, based on the 17 identified tree mortality events, Mitchell *et al.* (2014) used the intensity and duration of drought, in combination with heatwaves to define a common probabilistic climatic threshold for all vegetation types across Australia. They found that species in Australian ecosystems were resilient to the majority of historic climatic conditions but are likely to experience greater drought mortality risk by 2050. Such statistical approaches are powerful, but unless underpinned by extensive mortality data sets (e.g. Neumann *et al.* (2017)), they lack the sophistication to distinguish between regional, or even species behaviour (fundamentally limited by the climate data resolution, which is typically coarse). These statistical approaches also assume that the presentation of climate stresses that occurred in the past will be replicated in the future (i.e. with no change in the interaction between soil moisture, vapour pressure deficit (D), temperature and atmospheric carbon dioxide (Kelly *et al.*, 2016)) and that there is no systematic acclimation and/or adaptation by the vegetation as the climate changes.

Thus, despite numerous field and manipulation experiments leading to advances in our physiological understanding of the impact of drought, global-scale mortality thresholds remain elusive (Choat *et al.*, 2012; Mencuccini *et al.*, 2015). In places where we do not yet know the *in situ* mortality thresholds, we are unlikely to be able to link tree mortality to climatic water deficit metrics or hydraulic traits alone, limiting our ability to forecast drought impact globally. Consequently, we might opt for a more physiological approach that integrates climatic stress through the soil-plant-atmosphere continuum via a model. However, simulating the impact of water stress on vegetation function is a key weakness shared amongst land surface schemes used in climate models (Galiano *et al.*, 2010; Egea *et al.*, 2011;

Powell *et al.*, 2013; De Kauwe *et al.*, 2015b; Christoffersen et al. 2016; Ukkola *et al.*, 2016a) and very few approaches mechanistically link soil moisture stress and turnover of plant tissues (but see Xu *et al.*, 2016), or directly simulate drought-induced mortality.

Our goal in this study was to examine whether we can use this physiological understanding of drought mortality to make predictions at landscape scale. We embedded a representation of plant hydraulics into the Australian land surface model, CABLE (Community Atmosphere–Biosphere Land Exchange). We extend the model by incorporating the "second" drought phase (after stomata have closed), allowing water to continue to be lost via cuticular conductance (Choat *et al.*, 2018). We parameterised this new CABLE-Hydraulics based on a drought manipulation experiment on 12 woody species originating from a broad precipitation gradient (mean annual precipitation: 188-1125 mm yr^{-1}) across southeastern Australia (Li *et al.*, 2018). We then applied the new model at the landscape scale to make predictions of hydraulic failure due to drought in the Millennium (2000–2010) and "Big Dry" (2017–2019) droughts. We used our model simulations to identify if, where and when, species were most vulnerable to drought-induced mortality across South-East Australia (study area shown in Figure S3).

Methods

Model description

CABLE is a land surface scheme, which can be run offline with prescribed meteorological forcing (Wang *et al.*, 2011; De Kauwe *et al.*, 2015b; Ukkola *et al.*, 2016b; Decker *et al.*, 2017; Haverd *et al.*, 2018), or fully coupled (Pitman *et al.*, 2011; Lorenz *et al.*, 2014) within the Australian Community Climate Earth System Simulator (ACCESS, see http://www.accessimulator.org.au; Kowalczyk *et al.* (2013)).

CABLE simulates the carbon, energy and water fluxes at the land surface, representing the vegetation using a single layer, two-leaf (sunlit/shaded) canopy model (Wang & Leuning, 1998), with a detailed treatment of within-canopy turbulence (Raupach, 1994; Raupach *et al.*, 1997). In the model, soil water and heat conduction are numerically integrated over six discrete soil layers (4.6 m depth) following the Richards equation. The model groups vegetation globally into 11 plant functional types (PFTs). CABLE has the capacity to be run with an interactive biogeochemistry module (nitrogen and phosphorus) (Wang *et al.*, 2010) and vegetation demography model (Haverd *et al.*, 2014), but both of these were switched off for our simulations because leaf area index was prescribed (see below).

A complete description of the model can be found in Kowalczyk *et al.* (2006) and Wang *et al.* (2011). The model source code can be accessed freely after registration at https://trac.nci.org.au/trac/cable. In this paper we used CABLE revision 6134.

Simulating hydraulic failure

Following Xu *et al.* (2016), we introduced an augmented plant hydraulic module ("Desica") into CABLE to replace the default empirical representation of drought stress based on volumetric soil moisture content, weighted by the fraction of roots in each of CABLE's six soil layers (De Kauwe *et al.*, 2015b). Desica tracks water flow through the soil-plant-atmosphere continuum based on the gradient in water potentials between the leaf (Ψ_l, MPa), stem (Ψ_x, MPa) and the weighted average of the soil (Ψ_{sw}, MPa).

For each soil layer (i), we related the volumetric water content (θ, $m^3\ m^{-3}$) to soil water potential (Ψ_s, MPa) following Campbell (1974):

$$\Psi_{s,i} = \Psi_e \left(\frac{\theta}{\theta_{sat}} \right)^{-b} \quad (1)$$

where Ψ_e (MPa) is the air entry point water potential , θ_{sat} ($m^3\ m^{-3}$) is the soil volumetric moisture content at saturation and b (unitless) is the empirical pore size distribution index which approximates the slope of the soil-water retention curve (Clapp & Hornberger, 1978).

To obtain a representative value of whole root-zone Ψ_s, we weighted the average Ψ_s for each of the six soil layers by the weighted soil-to-root resistance to water uptake (R_s, MPa s $m^2\ m^{-3}$) of each layer (Williams *et al.*, 2001a; De Kauwe *et al.*, 2015b). Following Gardner (1960), for each soil layer, R_s is defined as:

$$R_{s,i} = \frac{ln(\frac{r_s}{r_r})}{2\pi l_r D K_{soil}} \quad (2)$$

where r_s is the mean distance between roots (m) (Williams et al. 2001a), r_r is the fine root radius (m) (Williams et al. 2001a), D is the depth of the soil layer (m) (Jackson et al. 1996), l_r is the fine root density ($m\ m^{-3}$) (Williams et al. 2001a) and K_{soil} is the soil hydraulic conductivity ($m^2\ s^{-1}\ MPa^{-1}$) which depends on soil texture and soil water content. The total below-ground soil-to-root resistance is calculated as the reciprocal of the summed inverses of each soil layer's resistance.

To solve the leaf (Ψ_l) and stem water potentials Ψ_x requires integration, which can lead to an instability due to the dependence on Ψ_l. Xu *et al.* (2016) proposed a simplification by treating Ψ_x as a constant ($\Psi_{x_{t-1}}$) by using the previous time step (Equation 5), which allows Ψ_l to be solved analytically. Similarly, the soil water potential is assumed to be a constant ($\Psi_{sw_{t-1}}$)

when calculating Ψ_x (Equation 8). Xu *et al.* (2016) argued that their simplifications did not result in large biases at the 10-minute timescale. Here, we followed their approach at the 30-minute timescale due to the limitations of the forcing data.

Ψ_l is solved as:

$$\Psi_l = \frac{(a_l \Psi_{l_{t-1}} + b_l) e^{(a\Delta t)} - b_l}{a_l} \quad (3)$$

where $\Psi_{l_{t-1}}$ is the leaf water potential from the previous time step (MPa), Δt is the timestep (30 minutes in this case), a_l and b_l are solved as:

$$a_l = \frac{-k_{xl}}{C_l} \quad (4)$$

$$b_l = \frac{\Psi_{x_{t-1}} k_{xl} - (\mathrm{LAI} \cdot E)}{C_l} \quad (5)$$

where k_{xl} is the conductance from the stem water store to the leaves (mmol m^{-2} s^{-1} MPa^{-1}), E is the transpiration flux from the canopy (mmol m^{-2} s^{-1}), C_l the leaf capacitance (mmol m^{-2} s^{-1} MPa^{-1}) scaled up by the canopy leaf area (LAI, m^2 m^{-2}).

Ψ_x is then calculated as:

$$\Psi_x = \frac{(a_x \Psi_{x_{t-1}} + b_x) e^{(a\Delta t)} - b_x}{a_x} \quad (6)$$

where $\Psi_{x_{t-1}}$ is the stem water potential from the previous time step. a_x and b_x are solved as:

$$a_x = \frac{-k_{sx}}{C_s} \qquad (7)$$

$$b_x = \frac{\Psi_{sw_{t-1}} k_{sx} - J_{sl}}{C_s} \qquad (8)$$

where $\Psi_{sw_{t-1}}$ is the weighted soil water potential from the previous timestep. k_{sx} is the conductance from the soil to the stem water store (mmol m^{-2} s^{-1} MPa^{-1}), which includes the weighted soil-to-root conductance to water uptake (i.e. 1 / R_s) and the conductance from the root surface to the stem water pool (assumed to be halfway between the roots and the leaves). C_s is stem capacitance (mmol m^{-2} s^{-1} MPa^{-1}) scaled up by the leaf area-to-sapwood area ratio (LA:SA), sapwood density (kg m^{-3}) and height (m). J_{sl} is the flux of water from the stem to the leaves (mmol m^{-2} s^{-1}), calculated as:

$$J_{sl} = \frac{(\Psi_l - \Psi_{l_{t-1}})C_l}{\Delta t} + (\mathrm{LAI} \cdot E) \qquad (9)$$

Xu *et al.* (2016) iteratively solved an optimal stomatal conductance model based on Ψ_l. Instead, we used a stomatal conductance model that assumes a sigmoidal sensitivity to Ψ_l (Tuzet *et al.*, 2003):

$$g_s = \max(g_{min}, 1.6 g_1 \frac{A_n}{C_s} f(\Psi_l)) \qquad (10)$$

where g_s (mol m^{-2} s^{-1}) is the stomatal conductance to water vapour, g_{min} is the water lost via cuticular conductance from internal stored water (Choat *et al.*, 2018; Blackman *et al.*, 2019), A_n is the net assimilation rate (μmol m^{-2} s^{-1}), C_s is the CO_2 concentration at the leaf surface (μmol mol^{-1}) and g_1 (unitless) is a fitted constant representing the slope of the sensitivity of g_s

to A_n (-). The factor of 1.6 converts from conductance to CO_2 to conductance to water vapour. $f(\Psi_l)$ is a sigmoidal function defined as:

$$f(\Psi_l) = \frac{1 + e^{(S_f \Psi_f)}}{1 + e^{(S_f(\Psi_f - \Psi_l))}} \qquad (11)$$

where S_f (MPa^{-1}) determines the shape of the response of g_s to Ψ_l and Ψ_f (MPa) is a reference water potential.

Xylem conductance (k_x) was assumed to decline via cavitation: *i.e.* a relative drop from a maximum value (the maximum plant hydraulic conductance, k_{plant}; mmol m^{-2} leaf s^{-1} MPa^{-1}) following a Weibull model as Ψ_x declines (Ogle, 2009):

$$\frac{k_x}{k_{plant}} = \left(\frac{100 - 50}{100}\right)^{p} \qquad (12)$$

where

$$p = \left(\frac{\Psi_x}{|P_{50}|}\right)^{\frac{|P_{50}|S_{50}}{V}} \qquad (13)$$

and

$$V = (50 - 100)\ln(1 - 50/100) \qquad (14)$$

where P_{50} is xylem pressure inducing 50% loss of hydraulic conductivity due to embolism (MPa) and S_{50} (% MPa^{-1}) is the slope of the percentage loss of hydraulic conductivity (PLC) at P_{50}.

We assume that cavitation can be fully recovered following rainfall (Xu *et al.*, 2016). We extend Xu *et al.* (2016) by allowing CABLE to track hydraulic failure until it reaches the critical threshold of hydraulic failure associated with mortality. To achieve this, we assume that following stomatal closure, Ψ_x continues to decrease as water is lost via g_{min} (Choat *et al.*, 2018; Blackman *et al.*, 2019). Previous work has shown a strong link between a threshold corresponding to an 88% loss of stem hydraulic conductance (P_{88}) and drought mortality (Urli *et al.*, 2013; Li *et al.*, 2015, 2018). Here, we do not equate P_{88} with mortality, but rather interpret it as indicative of the vegetation approaching a point of hydraulic stress likely to correspond to mortality, Ψ_{crit}. We make this distinction because each grid cell (~5 km^2) would contain a number of trees, not all of which would be dead. To bridge the gap from Ψ_{crit} to mortality would require stochastic approaches that are beyond the scope of the study.

Model simulations

New land-cover map

We replaced the standard vegetation land-cover map used in CABLE with a five-class land-cover map (Figure S4) derived from the National Vegetation Information System (NVIS, https://www.environment.gov.au/land/native-vegetation/national-vegetation-information-system). NVIS classifies the extent and distribution of vegetation types in Australian landscapes into 32 classes. We reclassified the vegetation classes that make up South-East Australia based on the drought manipulation experiments on 12 dominant tree species, so as to represent five major woody vegetation types (https://data.nsw.gov.au/data/dataset/4b6f1b3f-f33a-4e56-a6dd-5b052f28a361) in New South Wales, Australia (see below). Our five new vegetation classes (Figure S4) were: (i) rainforest (RF); (ii) wet sclerophyll forest (WSF); (iii) dry sclerophyll forest (DSF); (iv) grass woodland (GRW); and (v) semiarid woodland (SAW).

Model parameterisation

Each of the five new vegetation classes was parameterised based on the hydraulic and physiological traits measured in the drought manipulation experiments conducted by Li *et al.* (2018), Li *et al.* (2019) and Blackman *et al.* (2019). Full details are given by Li *et al.* (2018) but in brief, after 4 months of growth, seedlings of each species were transplanted to a polytunnel growth facility at Western Sydney University. Seedlings were placed into 25 l bags filled with native loamy sand top-soil. There were two drought phases: (i) plants were first dried until the point of visual wilting and then re-watered for 10 days to allow for full recovery; and then (ii) water was completely withheld to allow plants to use up all of their available water reserves. A full suite of hydraulic and physiological traits was measured during the second dry-down period.

Hydraulic traits measured on young plants grown under common conditions are assumed to reflect trait values of mature trees growing in the field. In the case of stem xylem cavitation resistance, there is evidence that this is true for *Eucalyptus* species, with P_{50} measured on the main stem axis of younger plants closely matching P_{50} of branches collected from mature trees in the field (Bourne *et al.*, 2017; Blackman *et al.*, 2019). Stem P_{50} also appears to have limited plasticity in response to growth environment (Lamy *et al.*, 2014) . Leaf hydraulic traits may be expected to vary more in response to growth environment and this variation could lead to bias in model output.

Species traits were averaged within vegetation classes as grouped by Li *et al.* (2018). Specifically for each vegetation class, we estimated values for P_{50}, k_{plant} (plant hydraulic conductance, mmol m^{-2} leaf s^{-1} MPa^{-1}), C_l, C_s, V_{cmax} (maximum carboxylation rate at 25 °C, μ mol m^{-2} s^{-1}), J_{max} (maximum rate of electron transport at 25 °C, μmol m^{-2} s^{-1}), g_1; g_{min} (mmol

296 m^{-2} s^{-1}), S_{50}, S_f (MPa^{-1}, assumed to be fixed) and Ψ_f. The key parameter values are shown in
297 Table 1.

298 To apply the model at the landscape scale we had to make several simplifying assumptions.
299 To scale up the measured branch capacitance and obtain an estimate of total C_s, we used
300 experimentally measured estimates of LA:SA and sapwood density (Table 1) and height
301 estimates from LiDAR data (Simard *et al.*, 2011). We estimated heights of 32 m, 29 m, 25 m,
302 11 m and 7 m for the RF, WSF, DSF, GRW and SAW vegetation classes based on the median
303 heights of pixels within each vegetation class derived from the Geoscience Laser Altimeter
304 System, LiDAR data (Simard *et al.*, 2011). Root biomass was prescribed based on the
305 measured fine root biomass at the Eucalyptus woodland Free Air CO_2 Enrichment research
306 facility in native Australian forest experiment – 832 g C m^{-2} (Jiang *et al.*, 2020) – and used to
307 calculate l_r in Equation 2. This biomass value is comparable to values used in previous
308 studies (Williams *et al.*, 2001b; Schwarz *et al.*, 2004; Fisher *et al.*, 2007; Hill *et al.*, 2011) but,
309 in reality, root biomass would vary spatially. We found that our single site model results were
310 insensitive to varying fine root biomass between 200 and 1000 g C m^{-2} (Transpiration Root
311 Mean Squared Error, RMSE < 1 W m^{-2}). Root density (0.5 g cm^{-3}) and root resistivity (25
312 MPa s g $mmol^{-1}$) were prescribed following Williams *et al.* (2001b) and Bonan *et al.* (2014),
313 respectively. Bonan *et al.* (2014) found their plant hydraulics model to be most sensitive to
314 root resistivity among the root parameters. CABLE-hydraulics, however, showed no notable
315 sensitivity to root resistivity (Transpiration Root Mean Squared Error, RMSE < 1 W m^{-2}),
316 even when assuming a value as high as 150 MPa s g $mmol^{-1}$.

317 In our model simulations, we also assumed that each 5 km^2 grid cell was only occupied by
318 trees with a leaf area prescribed based on satellite data. This assumption is unrealistic
319 (because a large proportion of South-East Australia is composed of a mixture of trees,

agricultural land and grasslands); we made it because we aimed to explore drought-induced tree mortality. As models (even dynamic vegetation models) do not realistically account for below-ground water competition (see Fisher et al. 2018 for a review of the state-of-the-art), our assumption is the same as running a tiled model (grid box divided into fractions of different surface type) and simply analysing the tree fraction. The model results are interpreted accordingly.

Model forcing

We performed offline simulations for South-East Australia (~400,000 km^2) using gridded, 30-minute meteorological forcing of precipitation, downward shortwave and longwave radiation, surface air temperature, surface specific humidity, surface wind speed, surface air pressure and atmospheric carbon dioxide concentration. We ran the model over the period 2000–2010 (Millennium Drought; spin-up 1995–1999) and 2017–2019 (Big Dry; spin-up 2011–2016) at a resolution of 0.05° (~5 km^2). The meteorological data were sourced from the Bureau of Meteorology's Australian Water Availability Project (AWAP) (Jones *et al.*, 2009) and the near-surface wind data of McVicar *et al.* (2008; McVicar, 2011). Data were downscaled from daily inputs to 3-hourly time steps using a weather generator (Haverd *et al.*, 2013) and then linearly interpolated to obtain 30-minute forcing. For the precipitation forcing, 30-minute data were obtained by first translating the 3-hourly rate to 30-minutes time slots and then assuming zero rainfall for the additional 30-minutes time slots. Wind data from McVicar (2011) were not available for 2019 so a monthly climatology from 2014-2018 was substituted.

CABLE was run with prescribed LAI based on a climatology (1999–2017) derived from the Copernicus LAI product, which is distributed by the Copernicus Global Land portal (http://land.copernicus.eu/global/). The Copernicus LAI product is derived from

343 SPOT/VEGETATION and PROBA-V data at 10-day intervals at a 0.01° (~1 km) spatial
344 resolution using a neural network approach. To force CABLE, we degraded the data from a
345 resolution of 0.01° to 0.05°. By prescribing LAI we avoid the need for a long model spin-up,
346 only requiring five years to stabilise the soil temperature and root-zone soil moisture.
347 Prescribing the LAI also avoids the assumption that the forest is in equilibrium with the
348 current climate, as would be the case had we spun up the model's carbon cycle. The model
349 was therefore spun up using five-year periods (repeating the meteorological forcing, 1995-
350 1999 and 2011-2016, see below).

351 Soil properties (e.g. texture, soil hydraulic and thermal characteristics) for CABLE were
352 based on the SoilGrids (Hengl *et al.*, 2017) data. Data were degraded using local area
353 averaging from 250m to 0.05° for simulations. We also tested the sensitivity of our results to
354 the 90m Soil and Landscape Grid of Australia soil dataset
355 (https://www.clw.csiro.au/aclep/soilandlandscapegrid) degraded to 0.05° (~5 km) but found
356 no significant impact arising from the choice of dataset. As is standard in CABLE, we
357 assumed vertically uniform soil texture based on the weighted average of the 2 m SoilGrids
358 data.

359 *Sensitivity experiment*

360 To better understand the resilience to drought conferred by hydraulic traits, we also carried
361 out a model sensitivity experiment. Starting from a wet soil profile and without further
362 precipitation, we asked: how long would it take for each vegetation class to reach Ψ_{crit}
363 (assumed to be P_{88})? For each of the five vegetation types, we sampled (5 samples) ±35% of
364 the measured trait averages for g_{min}, P_{50}, C_l and C_s. We also sampled between the interquartile
365 range (i.e. difference between 75th and 25th percentiles) LAI value, θ_{sat} and b found within

366 the geographical range of each vegetation class. Temperature was fixed to 35°C and a relative
367 humidity set to 10%. A temperature of 35°C is common in summers in South East Australia:
368 in New South Wales, the average maximum temperature during summer is 31°C and the 10
369 hottest summers on record all have days exceeding 40°C (Bureau of Meteorology;
370 http://www.bom.gov.au/).

371 For computational efficiency, we coupled the plant hydraulics module (Desica) to a big-leaf
372 canopy module (with the same coupled photosynthesis-stomatal conductance approach from
373 CABLE) and a single soil water "bucket" (of varying depth between 0.1 and 1 m), where the
374 only losses from the soil profile were assumed to be due to transpiration ($E=1.6g_sD$). In total,
375 we ran 140,625 simulations in the sensitivity experiment.

376 The sensitivity experiments were designed to examine the vegetations' tolerance to extreme
377 drought conditions but as the simulations use an imposed extreme climate and a simpler
378 representation of soil hydrology, the exact simulated day of Ψ_{crit} should be interpreted
379 cautiously. Instead, we were interested in the relative simulated differences between to Ψ_{crit}
380 for the vegetation classes.

381 Data sets used

382 Satellite data

383 To test whether our model realistically predicts where water stress occurred during the
384 Millennium Drought, we calculated anomaly maps (percent difference) using remote sensing
385 estimates of vegetation optical depth (VOD) and normalised difference vegetation index
386 (NDVI).

VOD data describes the attenuation of microwave wavelengths through the vegetation layer and has been assumed to be most sensitive to above-ground vegetation water content and changes in leaf/branch biomass (van Dijk *et al.*, 2013). We used two VOD datasets to quantify the change in the vegetation due to drought. For the Millennium drought, we calculated the average and greatest difference from a baseline average between 1993 and 1999, using a merged passive microwave VOD product (Liu *et al.*, 2011). For the Big Dry (2017-2018) we estimated an anomaly from a baseline between 2010 and 2016. In the latter case, we used the land parameter data record (LPDR) version 2 VOD product (Du *et al.*, 2017), which uses retrievals from the Advanced Microwave Scanning Radiometer for EOS (AMSR-E) and the Advanced Microwave Scanning Radiometer 2 (AMSR2). We used two different products because no single microwave sensor covers the entire period.

NDVI quantifies the photosynthetically active radiation that is absorbed by vegetation and so captures changes in foliar vegetation during periods of water stress. For the Millennium drought, we calculated the average and greatest difference from a baseline average between 1993 and 1999 (baseline chosen to match VOD). For the Big Dry (2017-2018), we estimated an anomaly from a baseline between 2010 and 2016. In each case, we used the NOAA Climate Data Record version 4 product based on the Advanced Very High Resolution Radiometer (AVHRR) sensor (Vermote, 2019).

In both remotely sensed estimates, we excluded the final summer period from our anomaly calculation for the Big Dry (2019), owing to the potential contamination due to fires in South-East Australia.

Climatic water deficit

A number of approaches have been used in the literature to quantify drought impact via a climatic water deficit. To explore the usefulness of these approaches, we calculated an estimate of climatic water deficit: precipitation minus potential evapotranspiration (P-PET). For the calculation of mean P-PET at 0.05° resolution, precipitation data was taken from AWAP and PET was calculated following Priestley & Taylor (1972) from AWAP monthly incoming shortwave radiation (converted to sunshine hours) and mean air temperature using the R package rstash (https://github.com/rhyswhitley/r_stash; Davis *et al.* (2017)).

Ozflux eddy covariance

To evaluate the new hydraulics module, we ran CABLE-Hydraulics at two woodland sites within the Australian eddy covariance network: the Wombat state forest (37.42°S, 144.09°E; Griebel *et al.* (2016)) and Tumbarumba (35.65°S, 148.15°E; Keith *et al.* (2012)) sites. We assumed that the Wombat site could be represented as a DSF and Tumbarumba as a WSF vegetation type. Those sites were chosen because the measurements records cover periods with significant drought. The CABLE outputs compared to half-hourly eddy covariance measurements of the exchange of carbon dioxide, energy, and water vapour obtained from OzFlux (http://www.ozflux.org.au/, last access: 26 April 2017). We used Level 6 gap-filled data following Isaac *et al.* (2017). Flux data were pre-processed using the FluxnetLSM R package Ukkola *et al.* (2017) and then screened to retain measured and good-quality gap-filled data.

Analysis code

All analysis code is freely available from

https://github.com/mdekauwe/SE_AUS_drought_risk_paper.git

Results

Sensitivity experiment

Figure 1 shows the time taken for each vegetation class to reach Ψ_{crit}, expressed as a histogram. Varying all the possible trait combinations leads to a marked overlap in distributions of the simulated day of Ψ_{crit}, with the exception of the SAW class. Despite this overlap, there is a notable separation in the peaks of the WSF and RF classes and the GRW class has a very broad upper tail, which overlaps with the SAW class. Our model results suggest that the WSF class was the most vulnerable and the least vulnerable was SAW. Perhaps counter-intuitively, the RF class emerges as more resilient than all classes except SAW (but note broad upper tail of GRW). This result is due to a combination of the very negative P_{50} (Table 1), which is the third most resistant among the five vegetation classes and the lowest g_{min} value, meaning that the rate of cuticular water loss is relatively low. Overall, g_{min}, LAI and P_{50} (in that order of importance) were the predictors that contributed most to vegetation resilience (assessed using partial residual plots; not shown). Finally, the overlapping distributions in the simulated day of Ψ_{crit}, imply that when embedded within CABLE, our model should predict gradients in Ψ_{crit} rather than sharp boundaries that follow vegetation class boundaries.

Drought simulation at eddy-flux sites

Figures 2 and 3 show two flux site-scale comparisons between observations of latent heat flux (LE), flux-derived gross primary productivity (GPP) and simulated fluxes by standard CABLE (Control) and the new CABLE-Hydraulics (Hydraulics) model. At both sites there is

452 evidence of pronounced water stress (shown by the gaps between rainfall events). These site-
453 scale simulations allow us to evaluate the new hydraulics model.

454 Introducing a representation of plant hydraulics leads to marked improvements in CABLE's
455 capacity to simulate carbon and water fluxes during periods of water stress. During the
456 periods of water stress, the hydraulics model approximately halves the error in the modelled
457 LE relative to the Control, whilst also improving the simulation of GPP. At Wombat (Figure
458 2), the RMSE in LE was reduced from 37 W m^{-2} to 20 W m^{-2} (Pearsons's correlation
459 coefficient, r: 0.61 vs 0.82) and at Tumbarumba (Figure 3), the RMSE was reduced from 56
460 W m^{-2} to 36 W m^{-2} (r: 0.31 vs 0.58). These improvements result from the replacement of the
461 empirical drought-stress function based on soil texture (Fig S5; Figures S6 and S7 show the
462 evolution of modelled water potentials at both sites) with two drought-stress modifiers based
463 on Ψ_l, Ψ_x and measured hydraulic traits (e.g. P_{50}). Whilst it is clear that the new hydraulics
464 could be improved further (i.e. the sensitivity in both the control and hydraulics model
465 relative to the control remains similar), it is important to note that these simulations have not
466 been tuned to any of the sites.

467 *Climatic water deficit*

468 Figure 4 shows the widely used climatic water deficit metric (P−PET) prior to (panel a) and
469 the difference (during the Millennium Drought minus prior, panel b). In an environment
470 where PET is always high (due to high solar radiation and temperature), this approach is of
471 limited value for inferring drought impact on the vegetation, as panel b show little
472 distinguishable difference (hence we do not show the Big Dry). These climatic deficit maps
473 (Figure 4) can be compared to the year-to-year rainfall decile maps, which show distinct
474 spatial patterns (Figure S1).

Contrasting these P−PET deficit maps with maps that depend on actual evapotranspiration (AET), as simulated via CABLE-Hydraulics during the Millennium drought (Figure 5a) and the Big Dry (Figure 5b), clearly highlights the spatially heterogeneous impact of the drought. Both maps show greater deficit inland (moving west), although the regions of greatest deficit differ in spatial location and magnitude between the droughts. Overall, the simulated water stress (lower P-AET) was noticeably greater throughout South-East Australia during the Big Dry compared to the Millennium Drought, particularly east of 145°E.

Simulated hydraulic failure

In the coastal regions, despite the simulated (P-AET) deficit due to the drought (cf. Figures 5a to 5b focussing on north of 32°S and south of 37°S), CABLE simulates no signs of approaching Ψ_{crit} (the xylem pressure inducing 88 % loss of hydraulic conductivity) at any point during either drought (Figures 6a,b). These predictions are consistent with the satellite anomaly maps (VOD and NDVI), which both suggest limited impact along the coast of South-East Australia (Average anomaly: Figures 7 and 8; Greatest anomaly: Figures S8 and S9). Moving west and inland, the impact of the Big Dry is more marked than that of the Millennium drought, with many regions approaching a greater maximum PLC ~40-50 % (145°E to 151°E). In both droughts, CABLE consistently simulates large areas that reach Ψ_{crit} (north of 35°S and west of 145°E). In those regions, CABLE-Hydraulics indicates that trees would be unlikely to survive those two most recent droughts. Figure S10 shows the timecourse of Ψ_{sw}, Ψ_{l} and Ψ_{x} for four representative pixels from the GRW and SAW vegetation classes during the Big Dry. As can be seen by comparing Figures S10c and S10d, greater LAI (Figure S10d, see also sensitivity experiment) and so higher losses via g_{min} leads to increased water stress for SAW pixels.

Comparing the regions of greatest drought impact according to the remote sensing data (Average anomaly: Figures 7 and 8; Greatest anomaly: Figures S8 and S9) to the maps of maximum PLC (Figure 6), there is a reasonable degree of spatial agreement. The regions of greatest drought impact in both the VOD and NDVI maps are also areas of significant (>50 %) PLC. The higher agreement between the PLC map and the NDVI data, may relate to our assumption of perfect recovery upon rewatering (see discussion). The NDVI data for the Big Dry (Figure 8b) shows a more marked decline in green canopy cover than the Millennium drought (Figure 8a) and this is broadly consistent with the PLC maps (Figure 6). CABLE does appear to miss the decline in NDVI south of 37°S; however, this feature is not evident in the VOD data (Figure 7b). Overall, CABLE simulates a more widespread impact due to drought than the satellite data but is qualitatively consistent in identifying the regions of greatest impact. It is worth noting that CABLE is simulating uniform tree cover throughout the domain, so the evaluation against the satellite data is only indicative of potential drought impact.

Figure 9 shows the PLC map as an average timeseries for each tree class, allowing us to visualise the point during the droughts at which CABLE simulated the greatest impact. In the Millennium Drought (Figure 9a), the impact was greatest for all vegetation classes during mid 2002 – mid 2003 and mid 2006 – mid 2007, which is consistent with the rainfall decile maps (Figure S1). There is an increasing accumulated level of drought impact (GRW and SAW) as illustrated by a year-on-year increase in PLC between 2003 and 2007 (Figure 9). For the Big Dry, Figure 9b, there is a worsening state of the vegetated land surface leading into the 2019–2020 austral spring/summer.

Sensitivity to soil moisture

PLC increases as soil water declines for the Millennium drought (Figure 10; Figure S11 shows the Big Dry). We can see that in both droughts the DSF, GRW and SAW classes had very low available soil moisture in their top four layers ($\theta < 0.17$ m^3 m^{-3}). For the DSF class this led to little increase in PLC, but by contrast the simulated PLC for the GRW exceeded 20% for a large number of pixels. Given the similarity in the parameterised traits (Table 1, see also Figure 1), these differences show the additional stress imposed by the climate, *e.g.* through temperature and vapour pressure deficit. This sensitivity to climate becomes more pronounced at low volumetric soil water content values (cf. GRW and SAW) when the total below-ground soil-to-root resistance (see Equation 2) is greatest and the Ψ_x and Ψ_l drop significantly diurnally, leading to higher PLC values. In our sensitivity experiment (Figure 1), we sampled the interquartile range of LAI found within the SAW vegetation class and matching expectations based on traits (Table 1), the SAW appeared more resilient than other classes. However, for a ~1 % of pixels within the SAW vegetation class, LAI values exceeded 1.5 m^2 m^2, which is likely to reflect non-tree contributions (cf. Figures S10c and S10d).

Discussion

Did trees die during the droughts?

Globally, Australia stands out with limited reports of recent widespread drought-induced tree mortality (Allen *et al.*, 2015). There are a number of studies that have historically documented drought-related tree mortality across Australia (Hopkins, 1973; Landsberg, 1985; Pook, 1986; Fensham *et al.*, 2009; Ross & Brack, 2015), but reports of mortality during the decadal Millennium Drought are surprisingly few (Keith *et al.*, 2012). This contrasts with recent droughts in the California and Texas, in which severe droughts were estimated to have killed 100 million and 300 million trees, respectively (Asner *et al.*, 2016; Moore *et al.*, 2016;

Service, 2016). Were tree deaths during the Millennium Drought simply not recorded? Or instead are Australian tree species exceptionally resilient to drought and did not approach critical hydraulic thresholds? For large areas of South-East Australia (that supports a large proportion of Australia's forests), CABLE-Hydraulics did not predict that the trees approached Ψ_{crit} in either drought (Figure 6). These results were qualitatively in spatial agreement with remote sensing estimates, noting that the remote sensing estimates do not show mortality (Average anomaly: Figures 7 and 8; Greatest anomaly: Figures S8 and S9). However, the model is likely to be too sensitive to water stress in the initial phase (stomatal closure) of drought response (Figures 2 and 3), and too insensitive in the second phase (cuticular water loss), where we do not have data to evaluate the model.

Our model did predict potential drought-induced mortality across the extremely arid regions in northwestern New South Wales (Fig. S3), but this result should be interpreted cautiously. To explore tree-related drought mortality, we assumed that trees were able to grow all across South-East Australia. In the northwestern region we are approaching the Simpson desert where Donohue *et al.* (2009) used a satellite-derived estimate of persistent tree cover (a proxy for where trees grow) for this region to indicate that no trees grow there. However, trees having the mallee growth form, characterised by multiple stems and a massive lignotuber, are present, but are patchily located and sometimes in close proximity to river features. It has been suggested that these mallee communities could be classified either as woodlands or as shrublands given their physiognomy, which appears to be uniquely Australian (Whittaker *et al.*, 1979). Thus, an alternative view of CABLE's prediction is that trees, as defined by the five simulated habitat types, *should* not be able to live there during a drought without additional water sources (e.g. groundwater).

Anecdotal and visual point-scale reports (e.g. the citizen science Dead Tree Detective project; https://biocollect.ala.org.au/acsa/project/index/77285a13-e231-49e8-b212-660c66c74bac) suggest extensive tree mortality during the Big Dry across South-East Australia. Much of this mortality was observed during significant heatwaves in summer 2019, a period that we were unable to examine in the remotely-sensed data owing to the extensive bushfires. These observations would appear to be odds with our model predictions for the Big Dry (Figure 6b). Our model simulations simulated broadly similar results between the two droughts we examined, where the emerging reports point to a greater impact from the shorter, more-intense Big Dry. This may imply that while we have improved simulation performance during the initial phase of drought response by incorporating hydraulic function, more data are needed to better constrain the second phase (see below). In situ measurements of leaf water potential, carbohydrates reserves, leaf shedding, vulnerability to cavitation (Ψ_{50}, Ψ_{88}) and capacitance, would be particularly valuable. In addition, the anecdotal observations of canopy death during the heatwaves indicate that we need to more closely examine interactions between drought and heatwaves (so-called compound events) and simulated vegetation function in future work.

Emerging reports of canopy death are yet to be verified: many eucalypts may appear dead due to total canopy defoliation following hydraulic failure *i.e.* they hit Ψ_{crit} and, yet the trees may not be dead, since many eucalypts, resprout following rain (Nolan *et al.*, 2014). Furthermore, trees may not die directly from drought, but due to many other factors that may be associated with drought (e.g. pests and pathogens) (Weed *et al.*, 2013). Thus, attempts to predict drought mortality may need to consider resprouting capacity as well as hydraulic failure.

Australian trees are likely to be among the first ecosystems to be exposed to extremes of climate (e.g. higher temperatures) under climate change and insight into ecosystem responses

591 to extremes may be disproportionately valuable (van der Horst *et al.*, 2019) to developing
592 theory for trees world-wide. Most studies that have explored responses to drought compare
593 measured hydraulic traits but ignore differences in local climate. Or put another way, studies
594 have evaluated vulnerability simply from the axis of sensitivity and not accounted for risk too.
595 Our results highlight the importance of integrating both traits and climate to gain insight into
596 mortality predictions across species. In our (experimentally constrained) model simulations,
597 the divergence in ecosystem flux trajectories towards Ψ_{crit} is greater within vegetation classes
598 than what the traits themselves would imply (cf. PLC map, Fig. 6 and Table 1).

599 *Hydraulics models in land surface models*

600 Poor model performance during periods of water stress (Powell *et al.*, 2013; Medlyn *et al.*,
601 2016; Ukkola *et al.*, 2016a) have led authors to argue that we require a more mechanistic
602 approach to determine the impact of water stress on vegetation function in models (Sperry &
603 Tyree, 1988; McDowell *et al.*, 2013; Zhou *et al.*, 2013; De Kauwe *et al.*, 2015a; Sperry *et al.*,
604 2017). It is plausible that model improvements could be achieved by replacing the widespread
605 empirical functions based on soil moisture availability and texture with more mechanistic
606 representations of plant hydraulics. A series of land surface schemes have successfully
607 demonstrated this point with recent model advancements (Bonan *et al.*, 2014; Christoffersen
608 *et al.*, 2016; Xu *et al.*, 2016; Kennedy *et al.*, 2019; Eller *et al.*, 2020; Sabot *et al.*, 2020).
609 However, to date, the focus has predominantly been on individual sites (but see Xu *et al.*,
610 2016) and integrating trait measurements into viable global parameterisations for land surface
611 models remains a key challenge (not least due to the lack of high spatiotemporal resolution
612 climate data). Current coupled climate models do not adequately represent legacy effects of
613 drought (e.g. turnover of plant tissues, instantaneous recovery, etc), including drought-
614 induced mortality. Recovery after drought is not likely to be instantaneous (Saatchi *et al.*,

2013; Wigneron *et al.*, 2020), as commonly assumed by models, implying that surface energy partitioning feedback on atmospheric processes may be in gross error, which may be particularly important in future projections.

In this study, we introduced a hydraulics model into the CABLE LSM and made landscape-scale (~400,000 km^2) predictions of drought-induced mortality (Ψ_{crit}) during the Millennium drought and Big Dry across South-East Australia. The new hydraulics model notably improved simulations of carbon and water fluxes at the site level (Figures 2 and 3). In making predictions of the evolution of xylem tension during drought we have significantly advanced the predictive capacity of one state-of-the-art LSM, opening new research avenues to simulate realistic predictions of drought-induced mortality.

Our hydraulics approach does have limitations that are pertinent for the LSM community to consider further. First, in order to produce realistic simulations of water potentials, we had to drive CABLE with 30-minute meteorological forcing, requiring us to use a weather generator. At a spatial resolution of 0.05° (~5 km^2), these forcing files become significantly larger than files typically used to run offline LSMs. Using a weather generator introduces a new set of biases, for example by muting the diurnal variability in meteorological forcing, which may in turn reduce the intensity of atmospheric drivers during periods of weather extremes.

Second, explicit representations of plant hydraulics require additional model parameters, not just the most widely available hydraulic trait, P_{50} (see Table 1). This is the most challenging limitation to LSMs adopting these hydraulics approaches. Where would appropriate parameters come from at the global scale? Particularly, as hydraulic traits have been shown to have similar distributions when re-interpreted not at the species level, but in PFTs more commonly used in LSMs (Konings & Gentine, 2017). Here, we were fortunate to be able to

use an existing drought manipulation experiment that considered a wide spectrum of species originating from a marked aridity gradient. In future work we plan to extend this approach, particularly to consider a wider range of species originating from mesic environments. An alternative approach that may reduce the parameterisation burden would be to move towards the new generation of stomatal optimisation models that also account for hydraulic function (Sperry *et al.*, 2017). For example, Sabot *et al.* (2020) recently demonstrated considerable promise applying one of these approaches at the ecosystem-scale, improving model predictions during European droughts. Sabot *et al.* (2020) also proposed a number of simplifications that would make an optimisation approach viable within LSMs.

We used a modified version of the Tuzet *et al.* (2003) stomatal model to limit stomatal conductance as a function of Ψ_l. This approach is attractive as it removes the requirement to assume a minimum Ψ_l (e.g. Williams *et al.*, 1996; Bonan *et al.*, 2014; Xu *et al.*, 2016), which requires that plants follow isohydric behaviour during water stress, contrary to the emerging literature indicating a broad spectrum of isohydric and anisohydric stomatal behaviour (Klein, 2014; Martin-StPaul, 2017). However, using the Tuzet *et al.* (2003) model approach is not without limitations: for example, Yang *et al.* (2019) recently showed it to simulate unrealistic declines in Ψ_l with increasing vapour pressure deficit, in contrast to experimental observations. This may also explain the discrepancy in sensitivity to water stress shown between model and observations in the flux evaluations (Figures 2 and 3).

Future directions

During the summer of 2019-2020, >5 million ha of forest burnt across South-East Australia (Nolan *et al.*, 2020). The preceding drought which began in 2017, likely played a key role in priming the land surface to burn, due to increased dry fuel litter (leaf and branch shedding). In

our first attempt at a hydraulics model for Australia we did not consider the mechanistic turnover of plant tissues, but this is clearly an important future research direction. Xu *et al.* (2016) and Trugman *et al.* (2019) demonstrated promise in dynamically linking leaf phenology to plant hydraulics. Establishing a link between plant hydraulics and leaf shedding (Wolfe *et al.*, 2016) may greatly improve current approaches used to predict the likelihood that the land surface will burn. Existing approaches (e.g. the McArthur Forest Fire Danger Index) make simplistic assumptions about litter and its dryness, meaning that they are over-dependent on fire weather (i.e. temperature-based) metrics.

Our model simulations did highlight (Figures 5c and 6b) marked impact of drought across the more mesic northeastern woodlands (forests) of New South Wales, consistent with some of the lowest rainfall totals on record. However, the coastal areas that burnt in the 2019-2020 fire season were not necessarily regions our model highlighted as locations that approached Ψ_{crit}. That is not to say that CABLE did not predict these regions were impacted by drought, but it did not simulate that the drought was extreme enough to induce Ψ_{crit}. Comparing the soil water content for the RF, WSF and DSF regions between the Millennium drought and the Big Dry, shows very similar patterns (cf. Figures 10 and Figures S11). Future model-based work may address the length and severity of water deficit that would be required for more mesic vegetation areas to reach Ψ_{crit}. This could prove important for future land management, particularly given that the Big Dry may have been broken by recent extensive rainfall across South-East Australia, meaning we may not witness water stress thresholds that induce mortality.

In our study we assumed that once stomata had closed ("first" drought phase), water continues to be lost at a significantly lower rate via g_{min} (a proxy for stomatal leakiness; "second" drought phase). Extensive measurements of g_{min} are still limited (see Duursma *et al.*,

2018 for a review) but some studies have suggested the rate of water loss may have a temperature dependency in some species (Bueno *et al.*, 2019), implying a potentially important interaction during drought. To make these model simulations viable at high-spatial resolution (~5 km), we had to make a series of simplifying assumptions (e.g. that there is xylem refilling (see D. *et al.*, 2018), or additional xylary resistance (see Brodribb & Holbrook, 2004), which require careful evaluation against ground-based data. To bridge this gap, plant water potentials during heatwaves and droughts would be particularly valuable to help constrain model predictions and further develop predictive capacity.

Acknowledgements

MDK, AJP, AMU, MM, MEBS and MR acknowledge support Australian Research Council (ARC) Centre of Excellence for Climate Extremes (CE170100023). MDK, PM, LC and AJP acknowledge support from the ARC Discovery Grant (DP190101823). MDK was also supported from the NSW Research Attraction and Acceleration Program. MEBS also acknowledges support from the UNSW Scientia PhD Scholarship Scheme. This work used eddy covariance data acquired from the OzFlux portal (http://data.ozflux.org.au/portal/home). We thank the National Computational Infrastructure at the Australian National University, an initiative of the Australian Government, for access to supercomputer resources. All data analysis and plots were generated using the Python language and the Matplotlib library.

Data Availability Statement

The model source code can be accessed freely after registration at https://trac.nci.org.au/trac/cable. All analysis code is freely available from:

706 https://github.com/mdekauwe/SE_AUS_drought_risk_paper.git. In this paper we used
707 CABLE revision 6134. All satellite data used in this manuscript are freely available.

708708

709709

710710

711 References

712 **Adams H, Zeppel M, Anderegg W, Hartmann H, Landhäusser S, Tissue D, Huxman T,**
713 **Hudson P, Franz T, Allen C *et al.* 2017**. A multi-species synthesis of physiological
714 mechanisms in drought-induced tree mortality. *Nature Ecology and Evolution* **1**: 1285–1291.

715 **Allen CD, Breshears DD, McDowell NG**. **2015**. On underestimation of global vulnerability
716 to tree mortality and forest die-off from hotter drought in the anthropocene. *Ecosphere* **6**:
717 art129.

718 **Anderegg WR, Anderegg LD, Kerr KL, Trugman AT**. **2019**. Widespread drought-induced
719 tree mortality at dry range edges indicates climate stress exceeds species' compensating
720 mechanisms. *Global change biology*.

721 **Anderegg WR, Kane JM, Anderegg LD**. **2013**. Consequences of widespread tree mortality
722 triggered by drought and temperature stress. *Nature Climate Change* **3**: 30–36.

Anderegg W, Schwalm C, Biondi F, Camarero JJ, Koch G, Litvak M, Ogle K, Shaw J, Shevliakova E, Williams A *et al.* 2015. Pervasive drought legacies in forest ecosystems and their implications for carbon cycle models. *Science* **349**: 528–532.

Arndt SK, Sanders GJ, Bristow M, Hutley LB, Beringer J, Livesley SJ. **2015**. Vulnerability of native savanna trees and exotic khaya senegalensis to seasonal drought. *Tree physiology* **35**: 783–791.

Asner GP, Brodrick PG, Anderson CB, Vaughn N, Knapp DE, Martin RE. **2016**. Progressive forest canopy water loss during the 2012–2015 california drought. *Proceedings of the National Academy of Sciences* **113**: E249–E255.

Bittencourt P, Oliveira R, Costa A da, Giles A, Coughlin I, Costa P, Bartholomew D, Ferreira L, Vasconcelos S, Barros F *et al.* 2020. Amazonian trees have limited capacity to acclimate plant hydraulic properties in response to long-term drought. *Global Change Biology*.

Blackman CJ, Li X, Choat B, Rymer PD, De Kauwe MG, Duursma RA, Tissue DT, Medlyn BE. **2019**. Desiccation time during drought is highly predictable across species of eucalyptus from contrasting climates. *New Phytologist* **224**: 632–643.

Bonan G, Williams M, Fisher R, Oleson K. **2014**. Modeling stomatal conductance in the earth system: Linking leaf water-use efficiency and water transport along the soil-plant-atmosphere continuum. *Geoscientific Model Development* **7**: 2193–2222.

Bourne AE, Creek D, Peters JM, Ellsworth DS, Choat B. **2017**. Species climate range influences hydraulic and stomatal traits in eucalyptus species. *Annals of Botany* **120**: 123–133.

Breshears DD, Cobb NS, Rich PM, Price KP, Allen CD, Balice RG, Romme WH, Kastens JH, Floyd ML, Belnap J *et al.* 2005. Regional vegetation die-off in response to global-change-type drought. *Proceedings of the National Academy of Sciences* **102**: 15144–15148.

Brodribb TJ, Holbrook NM. **2004**. Stomatal protection against hydraulic failure: A comparison of coexisting ferns and angiosperms. *New Phytologist* **162**: 663–670.

Bueno A, Alfarhan A, Arand K, Burghardt M, Deininger A-C, Hedrich R, Leide J, Seufert P, Staiger S, Riederer M. **2019**. Effects of temperature on the cuticular transpiration barrier of two desert plants with water-spender and water-saver strategies. *Journal of experimental botany* **70**: 1613–1625.

Campbell GS. **1974**. A simple method for determining unsaturated conductivity from moisture retention data. *Soil science* **117**: 311–314.

Carter JL, White DA. **2009**. Plasticity in the huber value contributes to homeostasis in leaf water relations of a mallee eucalypt with variation to groundwater depth. *Tree Physiology* **29**: 1407–1418.

Choat B, Brodribb TJ, Brodersen CR, Duur, Lopez R, Medlyn BE. **2018**. Triggers of tree mortality under drought. *Nature* **558**: 531–539.

Choat B, Jansen S, Brodribb TJ, Cochard H, Delzon S, Bhaskar R, Bucci SJ, Feild TS, Gleason SM, Hacke UG *et al.* 2012. Global convergence in the vulnerability of forests to drought. *Nature* **491**: 752–755.

Christoffersen BO, Gloor M, Fauset S, Fyllas NM, Galbraith DR, Baker TR, Kruijt B, Rowland L, Fisher RA, Binks OJ *et al.* 2016. Linking hydraulic traits to tropical forest function in a size-structured and trait-driven model (tfs v. 1-hydro). *Geoscientific Model Development* **9**: 4227.

Ciais P, Reichstein M, Viovy N, Granier A, Ogee J, Allard V, Aubinet M, Buchmann N, Bernhofer C, Carrara A *et al.* 2005. Europe-wide reduction in primary productivity caused by the heat and drought in 2003. *Nature* **437**: 529–533.

Clapp R, Hornberger G. 1978. Empirical equations for some soil hydraulic properties. *Water resources research* **14**: 601–604.

Collins M, Knutti R, Arblaster J, Dufresne J-L, Fichefet T, Friedlingstein P, Gao X, Gutowski WJ, Johns T, Krinner G *et al.* 2013. Long-term climate change: Projections, commitments and irreversibility. In: Climate change 2013-the physical science basis: Contribution of working group i to the fifth assessment report of the intergovernmental panel on climate change. Cambridge University Press, 1029–1136.

Cook BI, Ault TR, Smerdon JE. 2015. Unprecedented 21st century drought risk in the american southwest and central plains. *Science Advances* **1**: e1400082.

D. VM, S. SJ, M. LD, H. FE, G. AM, Yujie W, L. AWR. **2018**. A stomatal control model based on optimization of carbon gain versus hydraulic risk predicts aspen sapling responses to drought. *New Phytologist*.

Dai A. **2013**. Increasing drought under global warming in observations and models. *Nature Climate Change* **3**: 52–58.

Davis T, Prentice IC, Stocker B, Thomas R, Whitley R, Wang H, Evans B, Gallego-Sala A, Sykes M, Cramer W. **2017**. Simple process-led algorithms for simulating habitats (splash v. 1.0): Robust indices of radiation, evapotranspiration and plant-available moisture. *Geoscientific Model Development* **10**: 689–708.

De Kauwe MG, Kala J, Lin Y-S, Pitman AJ, Medlyn BE, Duursma RA, Abramowitz G, Wang Y-P, Miralles DG. **2015a**. A test of an optimal stomatal conductance scheme within the CABLE land surface model. *Geoscientific Model Development* **8**: 431–452.

De Kauwe M, Zhou S-X, Medlyn B, Pitman A, Wang Y-P, Duursma R, Prentice I. **2015b**. Do land surface models need to include differential plant species responses to drought? Examining model predictions across a mesic-xeric gradient in europe. *Biogeosciences* **12**: 7503–7518.

Decker M, Or D, Pitman A, Ukkola A. **2017**. New turbulent resistance parameterization for soil evaporation based on a pore scale model: Impact on surface fluxes in cable. *Journal of Advances in Modeling Earth Systems*.

Dijk AI van, Beck HE, Crosbie RS, Jeu RA, Liu YY, Podger GM, Timbal B, Viney NR. **2013**. The millennium drought in southeast australia (2001–2009): Natural and human causes

802 and implications for water resources, ecosystems, economy, and society. *Water Resources*
803 *Research* **49**: 1040–1057.

804 **Donohue RJ, McVICAR TR, Roderick ML**. **2009**. Climate-related trends in australian
805 vegetation cover as inferred from satellite observations, 1981–2006. *Global Change Biology*
806 **15**: 1025–1039.

807 **Du J, Kimball JS, Jones LA, Kim Y, Glassy JM, Watts JD**. **2017**. A global satellite
808 environmental data record derived from amsr-e and amsr2 microwave earth observations.
809 *Earth System Science Data* **9**: 791.

810 **Duursma RA, Blackman CJ, Lopéz R, Martin-StPaul NK, Cochard H, Medlyn BE**.
811 **2018**. On the minimum leaf conductance: Its role in models of plant water use, and ecological
812 and environmental controls. *New Phytologist* **0**.

813 **Egea G, Verhoef A, Vidale PL**. **2011**. Towards an improved and more flexible
814 representation of water stress in coupled photosynthesis–stomatal conductance models.
815 *Agricultural and Forest Meteorology* **151**: 1370–1384.

816 **Eller CB, Rowland L, Mencuccini M, Rosas T, Williams K, Harper A, Medlyn BE,**
817 **Wagner Y, Klein T, Teodoro GS *et al.* 2020**. Stomatal optimisation based on xylem
818 hydraulics (sox) improves land surface model simulation of vegetation responses to climate.
819 *New Phytologist* **n/a**.

820 **Fan Y, Miguez-Macho G, Jobbágy EG, Jackson RB, Otero-Casal C**. **2017**. Hydrologic
821 regulation of plant rooting depth. *Proceedings of the National Academy of Sciences*:
822 201712381.

823 **Fensham R, Holman J**. **1999**. Temporal and spatial patterns in drought-related tree dieback
824 in australian savanna. *Journal of Applied Ecology*: 1035–1050.

825 **Fensham R, Fairfax R, Ward D**. **2009**. Drought-induced tree death in savanna. *Global*
826 *Change Biology* **15**: 380–387.

827 **Fisher R, Williams M, COSTA D, Lola A, Malhi Y, Costa R da, Almeida S, Meir P**.
828 **2007**. The response of an eastern amazonian rain forest to drought stress: Results and
829 modelling analyses from a throughfall exclusion experiment. *Global Change Biology* **13**:
830 2361–2378.

831 **Fisher, RA, Koven, CD, Anderegg, WRL**, et al. 2018. Vegetation demographics in Earth
832 System Models: A review of progress and priorities. *Global Change Biol*. 24: 35–54.

833 **Galiano L, Martínez-Vilalta J, Lloret F**. **2010**. Drought-induced multifactor decline of scots
834 pine in the pyrenees and potential vegetation change by the expansion of co-occurring oak
835 species. *Ecosystems* **13**: 978–991.

836 **Gardner WR**. **1960**. Dynamic aspects of water availability to plants. *Soil science* **89**: 63–73.

837 **Godfree RC, Knerr N, Godfree D, Busby J, Robertson B, Encinas-Viso F**. **2019**.
838 Historical reconstruction unveils the risk of mass mortality and ecosystem collapse during
839 pancontinental megadrought. *Proceedings of the National Academy of Sciences*.

840 **Griebel A, Bennett LT, Metzen D, Cleverly J, Burba G, Arndt SK**. **2016**. Effects of
841 inhomogeneities within the flux footprint on the interpretation of seasonal, annual, and
842 interannual ecosystem carbon exchange. *Agricultural and forest meteorology* **221**: 50–60.

Haverd V, Raupach M, Briggs P, Canadell J, Isaac P, Pickett-Heaps C, Roxburgh S, Gorsel E van, Viscarra Rossel R, Wang Z. **2013**. Multiple observation types reduce uncertainty in australia's terrestrial carbon and water cycles. *Biogeosciences* **10**: 2011–2040.

Haverd V, Smith B, Nieradzik L, Briggs P. **2014**. A stand-alone tree demography and landscape structure module for earth system models: Integration with global forest data. *Biogeosciences* **11**: 2343–2382.

Haverd V, Smith B, Nieradzik L, Briggs PR, Woodgate W, Trudinger CM, Canadell JG. **2018**. A new version of the cable land surface model (subversion revision r4601) incorporating land use and land cover change, woody vegetation demography, and a novel optimisation-based approach to plant coordination of photosynthesis. *Geoscientific Model Development* **11**: 2995–3026.

Hengl T, Jesus JM de, Heuvelink GB, Gonzalez MR, Kilibarda M, Blagotić A, Shangguan W, Wright MN, Geng X, Bauer-Marschallinger B *et al.* 2017. SoilGrids250m: Global gridded soil information based on machine learning. *PLoS one* **12**.

Hill T, Williams M, Woodward F, Moncrieff J. **2011**. Constraining ecosystem processes from tower fluxes and atmospheric profiles. *Ecological Applications* **21**: 1474–1489.

Hopkins ER. **1973**. Eucalypt dieback inAustralia. In: C. MG, Idczak RM, eds. Victoria: Forests Comission, 1–16.

Horst SVJ van der, Pitman AJ, De Kauwe MG, Ukkola A, Abramowitz G, Isaac P. **2019**. How representative are fluxnet measurements of surface fluxes during temperature extremes? *Biogeosciences* **16**: 1829–1844.

Isaac P, Cleverly J, McHugh I, Van Gorsel E, Ewenz C, Beringer J. **2017**. OzFlux data: Network integration from collection to curation. *Biogeosciences* **14**: 2903–2928.

Jiang M, Medlyn BE, Drake JE, Duursma RA, Anderson IC, Barton CVM, Boer MM, Carrillo Y, Castañeda-Gómez L, Collins L *et al.* 2020. The fate of carbon in a mature forest under carbon dioxide enrichment. *Nature* **580**: 227–231.

Jiang M, Zaehle S, De Kauwe MG, Walker AP, Caldararu S, Ellsworth DS, Medlyn BE. **2019**. The quasi-equilibrium framework revisited: Analyzing long-term enrichment responses in plant–soil models. *Geoscientific Model Development* **5**: 2069–2089.

Jones DA, Wang W, Fawcett R. **2009**. High-quality spatial climate data-sets for australia. *Australian Meteorological and Oceanographic Journal* **58**: 233.

Jump AS, Ruiz-Benito P, Greenwood S, Allen CD, Kitzberger T, Fensham R, Martínez-Vilalta J, Lloret F. **2017**. Structural overshoot of tree growth with climate variability and the global spectrum of drought-induced forest dieback. *Global change biology* **23**: 3742–3757.

Keith H, Van Gorsel E, Jacobsen KL, Cleugh HA. **2012**. Dynamics of carbon exchange in a eucalyptus forest in response to interacting disturbance factors. *Agricultural and Forest Meteorology* **153**: 67–81.

Kelly JW, Duursma RA, Atwell BJ, Tissue DT, Medlyn BE. **2016**. Drought × co 2 interactions in trees: A test of the low-intercellular co 2 concentration (ci) mechanism. *New Phytologist* **209**: 1600–1612.

Kennedy D, Swenson S, Oleson KW, Fisher RA, Lawrence DM, Costa ACL da, Gentine P. **2019**. Implementing plant hydraulics in the community land model, version 5. *Journal of Advances in Modeling Earth Systems*.

Klein T. **2014**. The variability of stomatal sensitivity to leaf water potential across tree species indicates a continuum between isohydric and anisohydric behaviours. *Functional Ecology* **28**: 1313–1320.

Konings AG, Gentine P. **2017**. Global variations in ecosystem-scale isohydricity. *Global Change Biology* **23**: 891–905.

Kowalczyk E, Stevens L, Law R, Dix M, Wang Y, Harman I, Haynes K, Srbinovsky J, Pak B, Ziehn T. **2013**. The land surface model component of access: Description and impact on the simulated surface climatology. *Aust Meteorol Oceanogr J* **63**: 65–82.

Kowalczyk EA, Wang YP, Wang P, Law RH, Davies HL. **2006**. *The csiro atmosphere biosphere land exchange (CABLE) model for use in climate models and as an offline model*. CSIRO.

Lamy J-B, Delzon S, Bouche PS, Alia R, Vendramin GG, Cochard H, Plomion C. **2014**. Limited genetic variability and phenotypic plasticity detected for cavitation resistance in a m editerranean pine. *New Phytologist* **201**: 874–886.

Landsberg J. **1985**. Drought and dieback of rural eucalypts. *Austral Ecology* **10**: 87–90.

Li X, Blackman CJ, Choat B, Duursma RA, Rymer PD, Medlyn BE, Tissue DT. **2018**. Tree hydraulic traits are co-ordinated and strongly linked to climate-of-origin across a rainfall gradient.

Li X, Chris BJ, Peters JM, Choat B, Rymer PD, Medlyn BE, Tissue DT. **2019**. More than iso/anisohydry: Hydroscapes integrate plant water-use and drought tolerance traits in ten eucalypt species from contrasting climates. *Functional Ecology*.

Li S, Feifel M, Karimi Z, Schuldt B, Choat B, Jansen S. **2015**. Leaf gas exchange performance and the lethal water potential of five european species during drought. *Tree physiology* **36**: 179–192.

Liu YY, Jeu RA de, McCabe MF, Evans JP, Dijk AI van. **2011**. Global long-term passive microwave satellite-based retrievals of vegetation optical depth. *Geophysical Research Letters* **38**.

Lorenz R, Pitman A, Donat M, Hirsch A, Kala J, Kowalczyk E, Law R, Srbinovsky J. **2014**. Representation of climate extreme indices in the access1. 3b coupled atmosphere-land surface model. *Geoscientific Model Development* **7**: 545–567.

Martin-StPaul NK et a. **2017**. Plant resistance to drought depends on timely stomatal closure. *Ecology Letters*.

McDowell NG, Fisher RA, Xu C, Domec J, Hölttä T, Mackay DS, Sperry JS, Boutz A, Dickman L, Gehres N *et al.* 2013. Evaluating theories of drought-induced vegetation mortality using a multimodel–experiment framework. *New Phytologist*.

McVicar TR. **2011**. Near-surface wind speed for australia. V10. Data collection.

McVicar TR, Van Niel TG, Li LT, Roderick ML, Rayner DP, Ricciardulli L, Donohue RJ. **2008**. Wind speed climatology and trends for australia, 1975–2006: Capturing the stilling

924 phenomenon and comparison with near-surface reanalysis output. *Geophysical Research*
925 *Letters* **35**.

926 **Medlyn BE, De Kauwe MG, Zaehle S, Walker AP, Duursma RA, Luus K, Mishurov M,**
927 **Pak B, Smith B, Wang Y-P *et al.* 2016**. Using models to guide field experiments: A priori
928 predictions for the CO_2 response of a nutrient-and water-limited native eucalypt woodland.
929 *Global Change Biology* **22**: 2834–2851.

930 **Mencuccini M, Minunno F, Salmon Y, Martínez-Vilalta J, Hölttä T**. **2015**. Coordination
931 of physiological traits involved in drought-induced mortality of woody plants. *New*
932 *Phytologist* **in press**.

933 **Mitchell P, O'Grady A, Tissue D, Worledge D, Pinkard E**. **2014**. Co-ordination of growth,
934 gas exchange and hydraulics define the carbon safety margin in tree species with contrasting
935 drought strategies. *Tree physiology* **34**: 443–458.

936 **Moore GW, Edgar CB, Vogel JG, Washington-Allen RA, March RG, Zehnder R**. **2016**.
937 Tree mortality from an exceptional drought spanning mesic to semiarid ecoregions.
938 *Ecological Applications* **26**: 602–611.

939 **Mueller RC, Scudder CM, Porter ME, Talbot Trotter III R, Gehring CA, Whitham TG**.
940 **2005**. Differential tree mortality in response to severe drought: Evidence for long-term
941 vegetation shifts. *Journal of Ecology* **93**: 1085–1093.

942 **Myers BA, Neales T**. **1984**. Seasonal changes in the water relations of eucalyptus behriana f.
943 Muell. And e. Microcarpa (maiden) maiden in the field. *Australian Journal of Botany* **32**:
944 495–510.

945 **Nepstad DC, Tohver IM, Ray D, Moutinho P, Cardinot G**. **2007**. Mortality of large trees
946 and lianas following experimental drought in an amazon forest. *Ecology* **88**: 2259–2269.

947 **Neumann M, Mues V, Moreno A, Hasenauer H, Seidl R**. **2017**. Climate variability drives
948 recent tree mortality in europe. *Global change biology* **23**: 4788–4797.

949 **Nolan RH, Boer MM, Collins L, Resco de Dios V, Clarke H, Jenkins M, Kenny B,**
950 **Bradstock RA**. **2020**. Causes and consequences of eastern australia's 2019-20 season of
951 mega-fires. *Global change biology*.

952 **Nolan RH, Mitchell PJ, Bradstock RA, Lane PN**. **2014**. Structural adjustments in
953 resprouting trees drive differences in post-fire transpiration. *Tree physiology* **34**: 123–136.

954 **Ogle K**. **2009**. Hierarchical bayesian statistics: Merging experimental and modeling
955 approaches in ecology. *Ecological Applications* **19**: 577–581.

956 **Peñuelas J, Canadell J, Ogaya R**. **2011**. Increased water-use efficiency during the 20th
957 century did not translate into enhanced tree growth. *Global Ecology and Biogeography* **20**:
958 597–608.

959 **Phillips RP, Bernhardt ES, Schlesinger WH**. **2009**. Elevated CO_2 increases root exudation
960 from loblolly pine (pinus taeda) seedlings as an n-mediated response. *Tree Physiology* **29**:
961 1513–1523.

962 **Phillips OL, Van Der Heijden G, Lewis SL, López-González G, Aragão LE, Lloyd J,**
963 **Malhi Y, Monteagudo A, Almeida S, Dávila EA *et al.* 2010**. Drought–mortality
964 relationships for tropical forests. *New Phytologist* **187**: 631–646.

965 **Pitman A, Avila F, Abramowitz G, Wang Y, Phipps S, Noblet-Ducoudré N de**. **2011**.
966 Importance of background climate in determining impact of land-cover change on regional
967 climate. *Nature Climate Change* **1**: 472–475.

968 **Pook E**. **1986**. Canopy dynamics of eucalyptus maculata hook. IV. Contrasting responses to
969 two severe droughts. *Australian journal of botany* **34**: 1–14.

970 Powell TL, Galbraith DR, Christoffersen BO, Harper A, Imbuzeiro HMA, Rowland L,
971 **Almeida S, Brando PM, Costa ACL da, Costa MH *et al.* 2013**. Confronting model
972 predictions of carbon fluxes with measurements of amazon forests subjected to experimental
973 drought. *New Phytologist* **200**: 350–365.

974 **Priestley CHB, Taylor R**. **1972**. On the assessment of surface heat flux and evaporation
975 using large-scale parameters. *Monthly weather review* **100**: 81–92.

976 **Raupach M**. **1994**. Simplified expressions for vegetation roughness length and zero-plane
977 displacement as functions of canopy height and area index. *Boundary-Layer Meteorology* **71**:
978 211–216.

979 **Raupach M, Finkele K, Zhang L**. **1997**. SCAM (soil-canopy-atmosphere model):
980 Description and comparison with field data. *Aspendale, Australia: CSIRO CEM Technical*
981 *Report*: 81.

982 **Reichstein M, Bahn M, Ciais P, Frank D, Mahecha MD, Seneviratne SI, Zscheischler J,**
983 **Beer C, Buchmann N, Frank DC *et al.* 2013**. Climate extremes and the carbon cycle. *Nature*
984 **500**: 287–295.

985 **Ross C, Brack C**. **2015**. Eucalyptus viminalis dieback in the monaro region, nsw. *Australian*
986 *forestry* **78**: 243–253.

987 **Rowland L, Costa ACL da, Galbraith DR, Oliveira RS, Binks OJ, Oliveira AAR, Pullen**
988 **AM, Doughty CE, Metcalfe DB, Vasconcelos SS *et al.* 2015**. Death from drought in tropical
989 forests is triggered by hydraulics not carbon starvation. *Nature* **528**: 119–122.

990 **Ruiz-Benito P, Madrigal-Gonzalez J, Ratcliffe S, Coomes DA, Kändler G, Lehtonen A,**
991 **Wirth C, Zavala MA**. **2014**. Stand structure and recent climate change constrain stand basal
992 area change in european forests: A comparison across boreal, temperate, and mediterranean
993 biomes. *Ecosystems* **17**: 1439–1454.

994 **Ruthrof K, Matusick G, Hardy G**. **2015**. Early differential responses of co-dominant
995 canopy species to sudden and severe drought in a mediterranean-climate type forest. *Forests*
996 **6**: 2082–2091.

997 **Saatchi S, Asefi-Najafabady S, Malhi Y, Aragão L, Anderson L, Myneni R, Nemani R**.
998 **2013**. Persistent effects of a severe drought on amazonian forest canopy. *Proceedings of the*
999 *National Academy of Sciences* **110**: 565–570.

1000 **Sabot ME, De Kauwe MG, Pitman AJ, Medlyn BE, Verhoef A, Ukkola AM,**
1001 **Abramowitz G**. **2020**. Plant profit maximisation improves predictions of european forest
1002 responses to drought. *New Phytologist*.

1003 **Schwarz PA, Law BE, Williams M, Irvine J, Kurpius M, Moore D**. **2004**. Climatic versus
1004 biotic constraints on carbon and water fluxes in seasonality drought-affected ponderosa pine
1005 ecoystems, *Global Biogeochemical Cycles* **18**: GB4007, doi:10.1029/2004GB002234.

Service UF. **2016**. *USDA forest service pacific southwest region. Aerial detection surveys report: Summary for may 15–19 report no. Fseprd506698*. USDA Forest Service.

Simard M, Pinto N, Fisher JB, Baccini A. **2011**. Mapping forest canopy height globally with spaceborne lidar. *Journal of Geophysical Research: Biogeosciences* **116**: G04021.

Sperry JS, Tyree MT. **1988**. Mechanism of water stress-induced xylem embolism. *Plant Physiology* **88**: 581–587.

Sperry JS, Venturas MD, Anderegg WR, Mencuccini M, Mackay DS, Wang Y, Love DM. **2017**. Predicting stomatal responses to the environment from the optimization of photosynthetic gain and hydraulic cost. *Plant, Cell & Environment* **40**: 816–830.

Stoneman G. **1994**. Ecology and physiology of establishment of eucalypt seedlings from seed: A review. *Australian Forestry* **57**: 11–29.

Trenberth KE, Dai A, Van Der Schrier G, Jones PD, Barichivich J, Briffa KR, Sheffield J. **2014**. Global warming and changes in drought. *Nature Climate Change* **4**: 17–22.

Trugman A, Anderegg L, Wolfe B, Birami B, Ruehr N, Detto M, Bartlett M, Anderegg W. **2019**. Climate and plant trait strategies determine tree carbon allocation to leaves and mediate future forest productivity. *Global change biology*.

Tuzet A, Perrier A, Leuning R. **2003**. A coupled model of stomatal conductance, photosynthesis and transpiration. *Plant, Cell & Environment* **26**: 1097–1116.

Ukkola A, De Kauwe MG, Pitman AJ, Best MJ, Haverd V, M. D, G. A, Haughton N. **2016a**. Land surface models systematically overestimate the intensity, duration and

magnitude of seasonal-scale evaporative droughts. In review. *Environmental Research Letters* **11**: 104012.

Ukkola AM, Haughton N, De Kauwe MG, Abramowitz G, Pitman AJ. **2017**. FluxnetLSM R package (v1.0): A community tool for processing fluxnet data for use in land surface modelling. *Geoscientific Model Development* **10**: 3379–3390.

Ukkola AM, Pitman AJ, Decker M, De Kauwe MG, Abramowitz G, Kala J, Wang Y-P. **2016b**. Modelling evapotranspiration during precipitation deficits: Identifying critical processes in a land surface model. *Hydrology and Earth System Sciences* **20**: 2403–2419.

Urli M, Porté AJ, Cochard H, Guengant Y, Burlett R, Delzon S. **2013**. Xylem embolism threshold for catastrophic hydraulic failure in angiosperm trees. *Tree physiology* **33**: 672–683.

Vermote E. **2019**. NOAA climate data record (cdr) of avhrr surface reflectance, version 5.

Wang Y, Leuning R. **1998**. A two-leaf model for canopy conductance, photosynthesis and partitioning of available energy i::: Model description and comparison with a multi-layered model. *Agricultural and Forest Meteorology* **91**: 89–111.

Wang YP, Kowalczyk E, Leuning R, Abramowitz G, Raupach MR, Pak B, Gorsel E van, Luhar A. **2011**. Diagnosing errors in a land surface model (CABLE) in the time and frequency domains. *Journal of Geophysical Research: Biogeosciences (2005–2012)* **116**.

Wang YP, Law RM, Pak B. **2010**. A global model of carbon, nitrogen and phosphorus cycles for the terrestrial biosphere. *Biogeosciences* **7**: 2261–2282.

Weed AS, Ayres MP, Hicke JA. **2013**. Consequences of climate change for biotic disturbances in north american forests. *Ecological Monographs* **83**: 441–470.

Whittaker R, Niering W, Crisp M. **1979**. Structure, pattern, and diversity of a mallee community in new south wales. *Vegetatio* **39**: 65–76.

Wigneron J-P, Fan L, Ciais P, Bastos A, Brandt M, Chave J, Saatchi S, Baccini A, Fensholt R. **2020**. Tropical forests did not recover from the strong 2015–2016 el niño event. *Science advances* **6**: eaay4603.

Williams AP, Allen CD, Macalady AK, Griffin D, Woodhouse CA, Meko DM, Swetnam TW, Rauscher SA, Seager R, Grissino-Mayer HD *et al.* 2013. Temperature as a potent driver of regional forest drought stress and tree mortality. *Nature climate change* **3**: 292–297.

Williams M, Bond B, Ryan M. **2001a**. Evaluating different soil and plant hydraulic constraints on tree function using a model and sap flow data from ponderosa pine. *Plant, Cell &, Environment* **24**: 679–690.

Williams M, Law BE, Anthoni PM, Unsworth MH. **2001b**. Use of a simulation model and ecosystem flux data to examine carbon-water interactions in ponderosa pine. *Tree physiology* **21**: 287–298.

Williams M, Rastetter EB, Fernandes DN, Goulden ML, Wofsy SC, Shaver GR and. **1996**. Modelling the soil-plant-atmosphere continuum in a quercus-acer stand at harvard forest: The regulation of stomatal conductance by light, nitrogen and soil/plant hydraulic properties. *Plant, Cell and Environment* **19**: 911–927.

Wolfe BT, Sperry JS, Kursar TA. **2016**. Does leaf shedding protect stems from cavitation during seasonaldroughts? A test of the hydraulic fuse hypothesis. *New Phytologist* **212**: 1007–1018.

Xu X, Medvigy D, Powers JS, Becknell JM, Guan K. **2016**. Diversity in plant hydraulic traits explains seasonal and inter-annual variations of vegetation dynamics in seasonally dry tropical forests. *New Phytologist* **212**: 80–95.

Yang J, Duursma R, De Kauwe M, Kumarathunge D, Jiang M, Mahmud K, Gimeno T, Crous K, Ellsworth D, Peters J *et al.* 2019. Incorporating non-stomatal limitation improves the performance of leaf and canopy models at high vapour pressure deficit. *Tree Physiology* **39**: 1961–1974.

Zhou S, Duursma RA, Medlyn BE, Kelly JW, Prentice IC. **2013**. How should we model plant responses to drought? An analysis of stomatal and non-stomatal responses to water stress. *Agricultural and Forest Meteorology* **182-183**: 204–214.

Figure Captions

Figure 1: Probability density and histograms showing the time taken to reach the point of hydraulic failure (Ψ_{crit}) for each of the five vegetation classes in the absence of precipitation, with a constant air temperature of 35°C and a relative humidity of 10%. For each vegetation class, the (horizontal) spread in the time taken to reach hydraulic failure relates to resilience infered from sampling all possible photosynthetic (e.g. Vcmax), hydraulic (e.g. P_{50}) and structural (LAI) traits. The vegetation classes shown are: Rainforest (RAF), Wet sclerophyll forest (WSF), Dry sclerophyll forest (DSF), Grassy Woodland (GRW) and Semi-arid

1086 woodland (SAW). For each vegetation class, the curved line shows the fitted kernel density
1087 estimate (KDE).

1088 Figure 2: A comparison between fluxes simulated by the Control and Hydraulics model for
1089 gross primary productivity (GPP) and latent heat flux (LE) at the Wombat State Forest
1090 FLUXNET site during a pronounced period of water stress. The data have been smoothed
1091 with a 5-day moving window to aid visualisation.

1092 Figure 3: A comparison between fluxes simulated by the Control and Hydraulics model for
1093 gross primary productivity (GPP) and latent heat flux (LE) at the Tumbarumba FLUXNET
1094 site during a pronounced period of water stress. The data have been smoothed with a 5-day
1095 moving window to aid visualisation.

1096 Figure 4: Average climatic water deficit: precipitation (P) minus potential evapotranspiration
1097 (PET) (a) prior to the Millennium Drought (1990–2000) and (b) the difference: during the
1098 Millennium Drought minus prior for South-East Australia.

1099 Figure 5: Average climatic water deficit: precipitation (P) minus actual evapotranspiration
1100 (AET) (a) simulated by CABLE-hydraulics for (a) Millennium Drought (2000–2009) and (b)
1101 the Big Dry (2017–2019).

1102 Figure 6: Maximum percentage loss of hydraulic conductivity (%) simulated by CABLE
1103 during (a) the Millennium drought (2000–2009) and (b) the Big Dry (2017–2019) (panel b).
1104 Ψ_{crit} is the xylem pressure inducing a 88 % hydraulic conductivity.

1105 Figure 7: Remotely sensed map of the relative percentage difference between: (a) the mean
1106 summer (December–February) vegetation optical depth (VOD) during the Millennium

drought (2000–2009) relative to 1993–2000 and (b) the mean summer VOD during the Big Dry (2017–2018) relative to 1993–2016. Note we do not include the final summer 2019 due to the confounding impact of fires across South-East Australia.

Figure 8: Remotely sensed map of the relative percentage difference between: (a) the mean summer normalised difference vegetation index (NDVI) during the Millennium drought (2000–2009) relative to 1993–2000 and (b) the mean summer NDVI during the Big Dry (2017– 2018) relative to 1993–2016. Note we do not include summer 2019 due to the confounding impact of fires across South-East Australia.

Figure 9: Timeseries of the percentage loss of hydraulic conductivity (%) for each of the five vegetation classes during (a) the Millennium drought and (b) Big Dry. For each vegetation class, the line shows the spatial average across all pixels. The vegetation classes shown are: Rainforest (RAF), Wet sclerophyll forest (WSF), Dry sclerophyll forest (DSF), Grassy Woodland (GRW) and Semi-arid woodland (SAW).

Figure 10: Sensitivity of percentage loss of hydraulic conductivity (%) to soil water availability in the top four soil layers (0.64 m, 80% of roots) for each vegetation class during the Millennium drought. The vegetation classes shown are: Rainforest (RAF), Wet sclerophyll forest (WSF), Dry sclerophyll forest (DSF), Grassy Woodland (GRW) and Semi-arid woodland (SAW). Ψ_{crit} is the xylem pressure inducing a 88 % hydraulic conductivity.

Supplementary Figure 1: South-East Australia's July to June annual rainfall during the Millennium drought (2000–2009) relative to historic records (1900–2018). Maps show each year's rainfall ranked against historic records expressed as a percentile.

Supplementary Figure 2: South-East Australia's July to June annual rainfall during the Big Dry (2016–2018) relative to historic records (1900–2018). Maps show each year's rainfall ranked against historic records expressed as a percentile.

Supplementary Figure 3: Study area in South-East Australia.

Supplementary Figure 4: New tree landcover map for South-East Australia, classified from the National Vegetation Information System's distribution of vegetation types in Australian landscapes. The legend shows: Rainforest (RAF), Wet sclerophyll forest (WSF), Dry sclerophyll forest (DSF), Grassy Woodland (GRW) and Semi-arid woodland (SAW).

Supplementary Figure 5: Water stress modifiers used in CABLE shown as: (a) a function of volumetric soil moisture content in the Control model and (b) (leaf and stem) water potential in the Hydraulics model. In the Control model, the water stress modifier limits canopy gas exchange, whereas in the hydraulics model Ψ_l limits stomatal conductance as a function of leaf water potential and Ψ_x limits whole-plant hydraulic conductance as a function of stem water potential. In the Control model, the water stress sensitivity is shown for a sand soil and in the Hydraulics model, the sensitivities are shown for the wet sclerophyll forest vegetation class.

Supplementary Figure 6: Modelled pre-dawn weighted soil (Ψ_{sw}), midday leaf (Ψ_l) and midday stem (Ψ_x) water potentials at the Wombat State Forest FLUXNET site during a pronounced period of water stress.

Supplementary Figure 7: Modelled pre-dawn weighted soil (Ψ_{sw}), midday leaf (Ψ_l) and midday stem (Ψ_x) water potentials at the Tumbarumba FLUXNET site during a pronounced period of water stress.

Supplementary Figure 8: Remotely sensed map of the relative percentage difference between: (a) the lowest summer (December–February) vegetation optical depth (VOD) during the Millennium drought (2000–2009) relative to 1993–2000 and (b) the mean summer VOD during the Big Dry (2017–2018) relative to 1993–2016. Note we do not include the final summer 2019 due to the confounding impact of fires across South-East Australia.

Supplementary Figure 9: Remotely sensed map of the relative percentage difference between: (a) the lowest summer normalised difference vegetation index (NDVI) during the Millennium drought (2000–2009) relative to 1993–2000 and (b) the mean summer NDVI during the Big Dry (2017–2018) relative to 1993–2016. Note we do not include summer 2019 due to the confounding impact of fires across South-East Australia.

Supplementary Figure 10: Modelled pre-dawn weighted soil (Ψ_{sw}), pre-dawn stem (Ψ_x) and midday leaf (Ψ_l) water potentials for two representative Grassy Woodland (GRW) (panels a and b) pixels and two representative Semi-arid woodland (SAW) (panels c and d) pixels during the Big Dry (2016–2019). Note the difference in trajectories between panels c and d relates to differences in leaf area index: 0.22 $m^2 m^{-2}$ (c) vs 1.6 $m^2 m^{-2}$ (d).

Supplementary Figure 11: Sensitivity of percentage loss of hydraulic conductivity (%) to soil water availability in the top four soil layers (0.64 m, 80% of roots) for each vegetation class during the Big Dry. The vegetation classes shown are: Rainforest (RAF), Wet sclerophyll forest (WSF), Dry sclerophyll forest (DSF), Grassy Woodland (GRW) and Semi-arid woodland (SAW). Ψ_{crit} is the xylem pressure inducing a 88 % hydraulic conductivity.

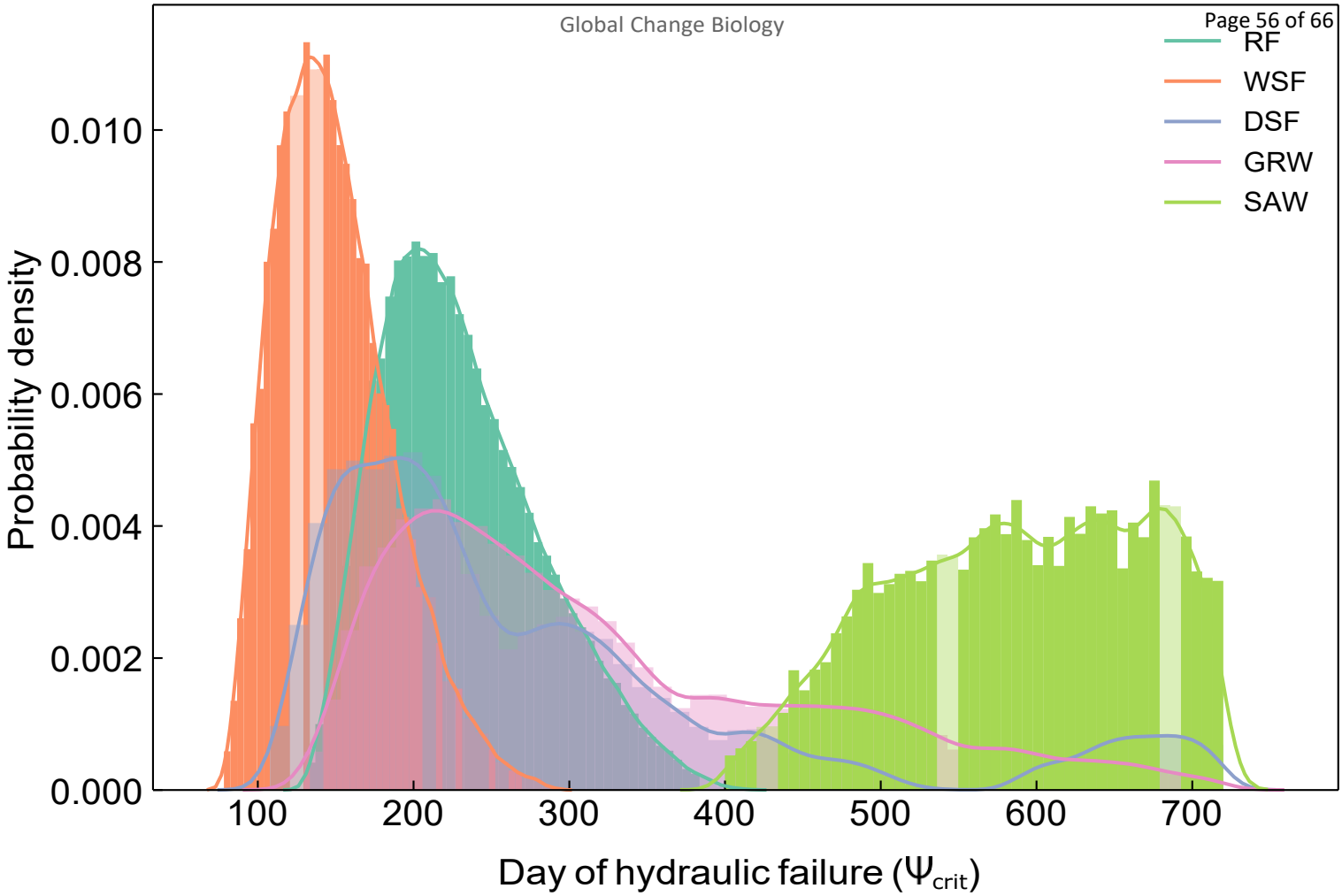
RF
WSF
DSF
GRW
SAW
Probability density
0.010
0.008
0.006
0.004
0.002
0.000
100
200
300
400
500
600
700
Day of hydraulic failure (Ψ_{crit})

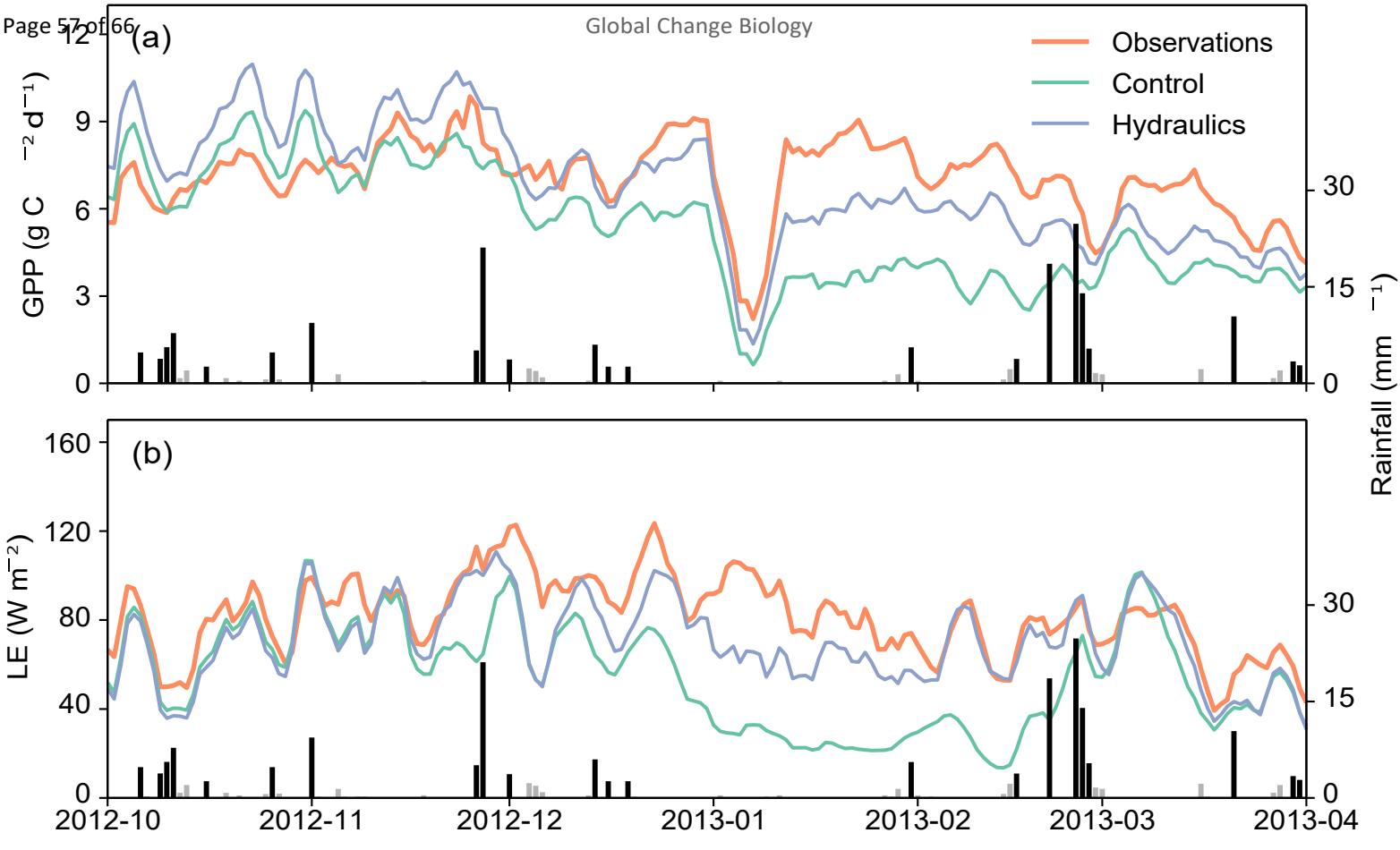
(a)
(b)
Observations
Control
Hydraulics
GPP (g C m^{-2} d^{-1})
LE (W m^{-2})
Rainfall (mm d^{-1})
0
3
6
9
12
40
80
120
160
15
30
2012-10
2012-11
2012-12
2013-01
2013-02
2013-03
2013-04

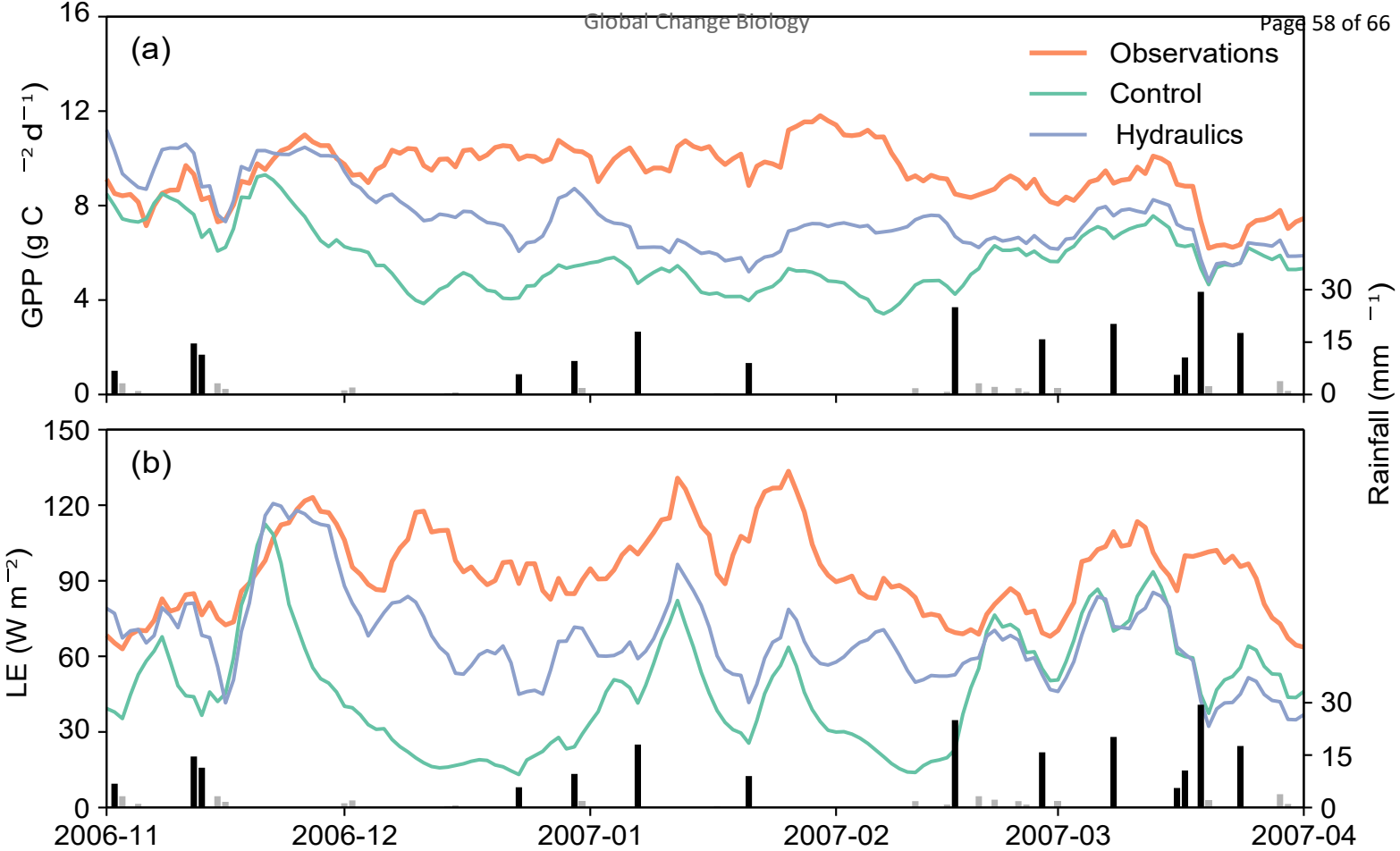
(a)
Observations
Control
Hydraulics
GPP (g C m^{-2} d^{-1})
Rainfall (mm)
(b)
LE (W m^{-2})
2006-11
2006-12
2007-01
2007-02
2007-03
2007-04

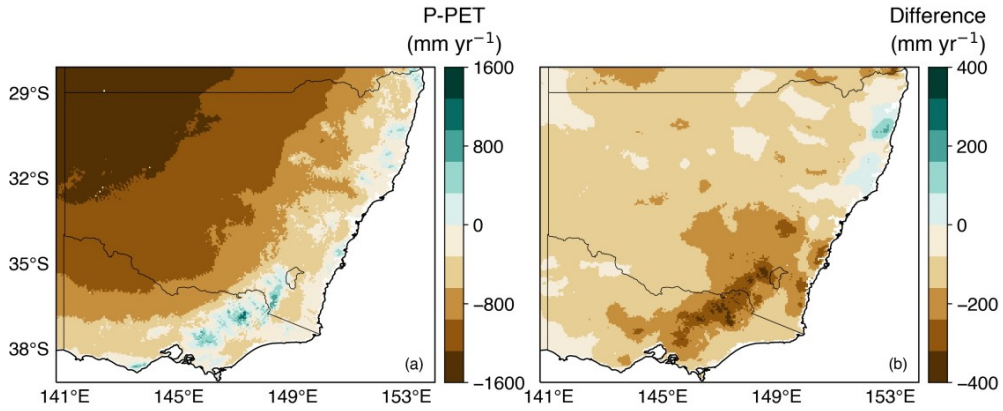

Figure 4: Average climatic water deficit: precipitation (P) minus potential evapotranspiration (PET) (a) prior to the Millennium Drought (1990–2000) and (b) the difference: during the Millennium Drought minus prior for South-East Australia.

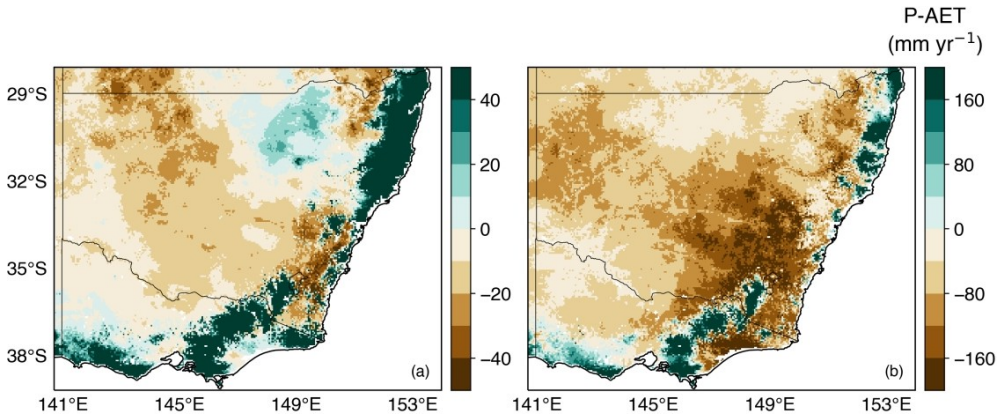

Figure 5: Average climatic water deficit: precipitation (P) minus actual evapotranspiration (AET) (a) simulated by CABLE-hydraulics for (a) Millennium Drought (2000–2009) and (b) the Big Dry (2017–2019).

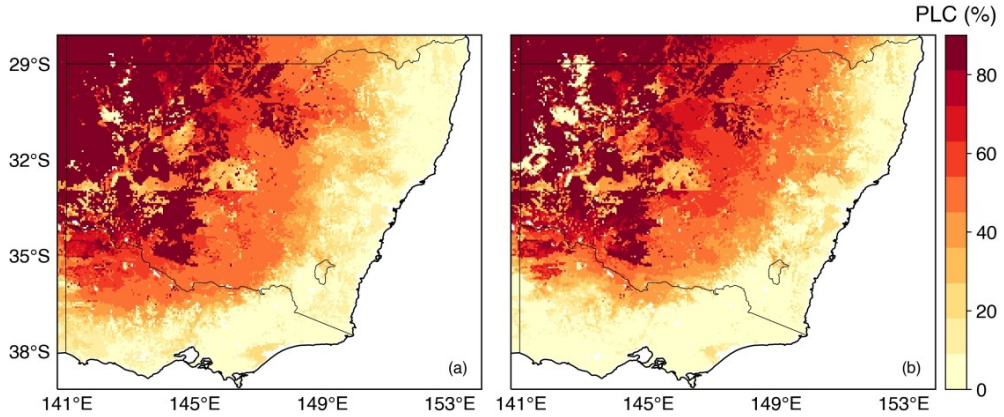

Figure 6: Maximum percentage loss of hydraulic conductivity (%) simulated by CABLE during (a) the Millennium drought (2000–2009) and (b) the Big Dry (2017–2019) (panel b). Ψcrit is the xylem pressure inducing a 88 % hydraulic conductivity.

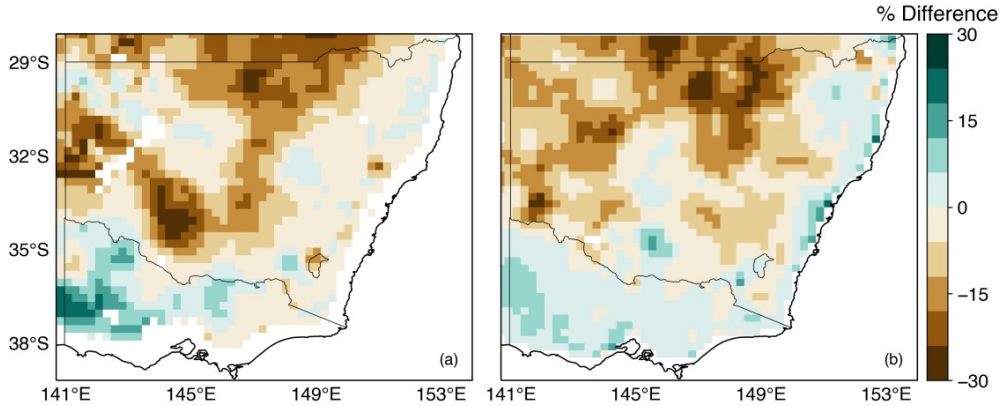

Figure 7: Remotely sensed map of the relative percentage difference between: (a) the mean summer (December–February) vegetation optical depth (VOD) during the Millennium drought (2000–2009) relative to 1993–2000 and (b) the mean summer VOD during the Big Dry (2017–2018) relative to 1993–2016. Note we do not include the final summer 2019 due to the confounding impact of fires across South-East Australia.

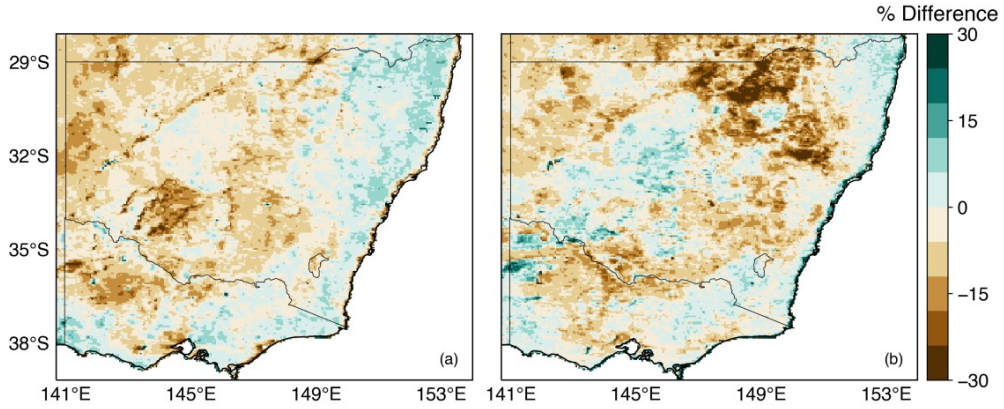

Figure 8: Remotely sensed map of the relative percentage difference between: (a) the mean summer normalised difference vegetation index (NDVI) during the Millennium drought (2000–2009) relative to 1993–2000 and (b) the mean summer NDVI during the Big Dry (2017– 2018) relative to 1993–2016. Note we do not include summer 2019 due to the confounding impact of fires across South-East Australia.

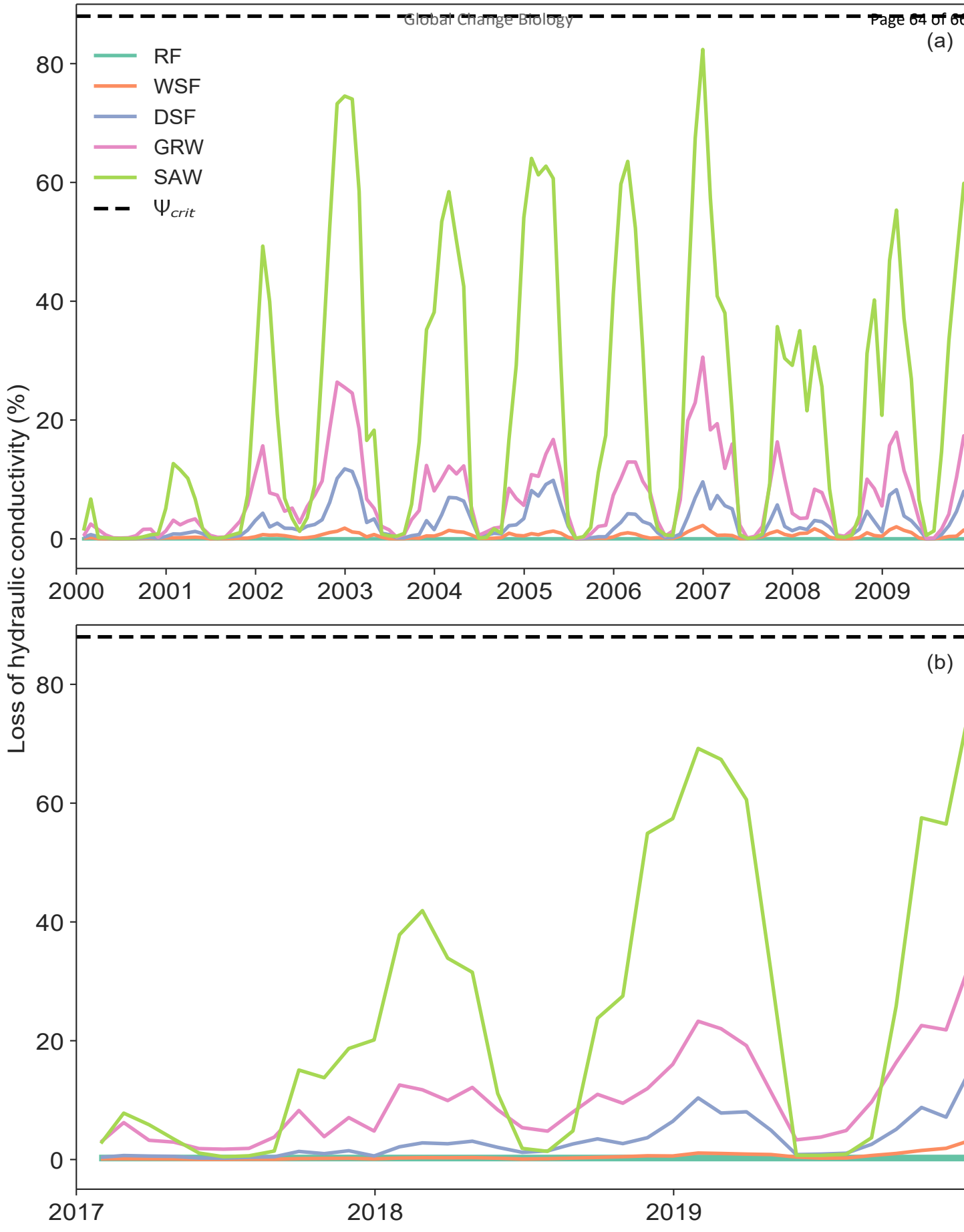
(a)
RF
WSF
DSF
GRW
SAW
Ψcrit
Loss of hydraulic conductivity (%)
0
20
40
60
80
2000
2001
2002
2003
2004
2005
2006
2007
2008
2009
(b)
0
20
40
60
80
2017
2018
2019

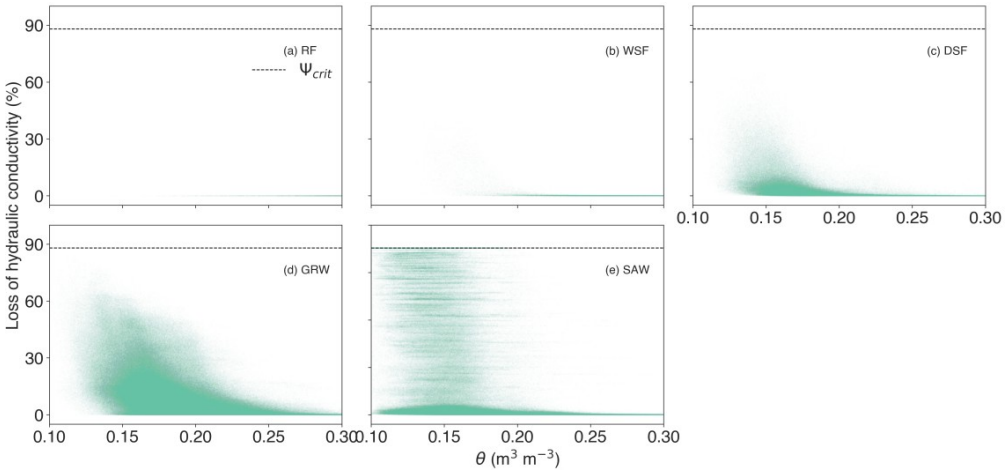

Figure 10: Sensitivity of percentage loss of hydraulic conductivity (%) to soil water availability in the top four soil layers (0.64 m, 80% of roots) for each vegetation class during the Millennium drought. The vegetation classes shown are: Rainforest (RAF), Wet sclerophyll forest (WSF), Dry sclerophyll forest (DSF), Grassy Woodland (GRW) and Semi-arid woodland (SAW). Ψcrit is the xylem pressure inducing a 88 % hydraulic conductivity.

	Definitions	Units	RF	WSF	DSF	GRW	SAW
g_1	Stomatal slope	-	4.2	3.2	4.8	4.8	5.1
g_{min}	Cuticular conductance	mmol m^{-2} s^{-1}	0.25	0.65	0.7	0.65	0.8
V_{cmax}	Value of V_{cmax} at 25 °C	μmol m^{-2} s^{-1}	44.1	84.9	75.6	62.3	92.8
J_{max}	Value of J_{max} at 25 °C	μmol m^{-2} s^{-1}	73.6	141.7	126.3	104.1	154.9
Ψ_f	Reference water potential	MPa	-2	-2.5	-1.7	-3.4	-3.7
S_f	Shape of response to Ψ_l	MPa^{-1}	2	2	2	2	2
k_{plant}	Plant hydraulic conductance	mmol m^{-2} MPa^{-1} leaf s^{-1}	2.3	1.6	2.4	2.2	2.9
S_{50}	Slope of the percentage loss of hydraulic conductivity	% MPa^{-1}	74.3	35.3	30.5	26.7	17.8
P_{50}	Water potential at 50% loss of hydraulic conductivity	MPa	-4.3	-3	-3.5	-4.5	-7.1
C_l	Leaf capacitance	mmol m^{-2} s^{-1} MPa^{-1}	659.1	342.9	349.2	405.1	509.1
C_s	Stem capacitance	mmol m^{-2} s^{-1} MPa^{-1}	8819.2	53266.1	26255.4	32508.6	11598.5
LA:SA	Leaf area-to-sapwood area ratio	m^2 m^{-2}	10000.0	9434.7	7908.6	6139.2	2556.9
WD	Sapwood density	kg m^{-3}	540.0	355.0	460.0	436.7	613.3

Table 1: Summary of vegetation type parameter values. The five vegetation types are: rainforest (RF); wet sclerophyll forest (WSF); dry sclerophyll forest (DSF); grass woodland (GRW); and semiarid woodland (SAW). Values shown are species averages based on Li *et al.* (2018), except for S_f, which was assumed to be fixed and the LA:SA for the RF class which was assumed to be 10,000 m^2 m^{-2}.